Journal of Biomolecular NMR (2005) 32: 309–328
DOI 10.1007/s10858-005-1195-4


*Article*

# Triple-resonance methods for complete resonance assignment of aromatic protons and directly bound heteronuclei in histidine and tryptophan residues

Frank Löhr*, Vladimir V. Rogov, Meichen Shi, Frank Bernhard & Volker Dötsch
*Institute of Biophysical Chemistry, Centre for Biomolecular Magnetic Resonance, Johann Wolfgang Goethe-University, Frankfurt am Main, Biozentrum N230, 1. OG, Marie Curie-Strasse 9, D-60439, Frankfurt, Germany*

Received 26 May 2005; Accepted 11 July 2005

*Key words:* amino acid type-selectivity, CC–TOCSY, hCdc5, multiple-relay, protein sequence specific assignments, RcsC-PR

**Abstract**

A set of three experiments is described which correlate aromatic resonances of histidine and tryptophan residues with amide resonances in $^{13}C/^{15}N$-labelled proteins. Provided that backbone $^{1}H$ and $^{15}N$ positions of the sequentially following residues are known, this results in sequence-specific assignment of histidine $^{1}H^{\delta 2}/^{13}C^{\delta 2}$ and $^{1}H^{\varepsilon 1}/^{13}C^{\varepsilon 1}$ as well as tryptophan $^{1}H^{\delta 1}/^{13}C^{\delta 1}$, $^{1}H^{\zeta 2}/^{13}C^{\zeta 2}$, $^{1}H^{\eta 2}/^{13}C^{\eta 2}$, $^{1}H^{\varepsilon 3}/^{13}C^{\varepsilon 3}$, $^{1}H^{\zeta 3}/^{13}C^{\zeta 3}$ and $^{1}H^{\varepsilon 1}/^{15}N^{\varepsilon 1}$ chemical shifts. In the reverse situation, these residues can be located in the $^{1}H$–$^{15}N$ correlation map to faciliate backbone assignments. It may be chosen between selective versions for either of the two amino acid types or simultaneous detection of both with complete discrimination against phenylalanine or tyrosine residues in each case. The linkages between δ-proton/carbon and the remaining aromatic as well as backbone resonances do not rely on through-space interactions, which may be ambiguous, but exlusively employ one-bond scalar couplings for magnetization transfer instead. Knowledge of these aromatic chemical shifts is the prerequisite for the analysis of NOESY spectra, the study of protein–ligand interactions involving histidine and tryptophan residues and the monitoring of imidazole protonation states during pH titrations. The new methods are demonstrated with five different proteins with molecular weights ranging from 11 to 28 kDa.

## Introduction

Sequence-specific aromatic ring $^{1}H$ and $^{13}C$ resonance assignments are not usually achieved with the standard set of heteronuclear *J*-correlation techniques (Bax and Grzesiek, 1993; Kay, 1995; Cavanagh et al., 1996) applied to isotopically enriched proteins. Nevertheless, their knowledge is of vital importance for an accurate determination of solution structures by NMR since aromatic residues are often located in the hydrophobic core of proteins and therefore involved in many long-range NOE contacts. In addition, histidines frequently occur at the active site of enzymes and its imidazole ring chemical shifts are potential reporters of its protonation state, tautomeric structure, solvent accessibility or the existence of hydrogen-bonds.

The 'bottleneck' for the sequence-specific assignment of aromatic resonances is to obtain the connectivity across the quarternary γ-carbon

*To whom correspondence should be addressed. E-mail: murph@bpc.uni-frankfurt.de

which devides the $^{1}H$ scalar coupling network into two separate spin-systems. In favourable cases they can by linked via intraresidual through-space interactions between ring protons and previously assigned α- or β-protons (Wagner and Wüthrich, 1982; Billeter et al., 1982; Wüthrich, 1986). For larger proteins, it may however be difficult to obtain complete assignments because of a high density of NOEs or a poor dispersion of aromatic $^{1}H$ chemical shifts. Relying on one-bond carbon–carbon couplings, experiments such as HCCH–COSY (Kay et al., 1990, Bax et al., 1990a), HCCH–TOCSY (Bax et al., 1990b) or HC(CCO)NH–TOCSY (Montelione et al., 1992; Logan et al., 1993; Grzesiek et al., 1993) are routinely applied for side-chain assignments, but here they offer no remedy because they are not designed for a transfer between the β- and γ-carbon spins of aromatic side chains. For the first time the problem was overcome by Yamazaki et al. (1993), who introduced (Hβ)Cβ(CγCδ)Hδ and (Hβ)Cβ(CγCδ Cε)Hε pulse sequences providing exclusively scalar coupling-based correlations between β-carbons and ring protons. Further improvements have been obtained by replacing the CC–COSY like transfer steps between β- and aromatic carbons of the latter sequences either by an audio-modulated spin lock field (Grzesiek and Bax, 1995) or by tailored TOCSY (Carlomagno et al., 1996). Recently, Peti et al. (2004) were able to show that the aliphatic–aromatic transfer is possible with a HCCH–TOCSY sequence using a microcoil flow-through probe which allows for the application of very high $^{13}C$ spin-lock fields.

Another approach involves recording of $^{13}C^{\gamma}$ chemical shifts in order to establish connectivities between aromatic and β-protons via common correlations with the latter in a single (Pelton et al., 1993) or at least two separate experiments (Löhr and Rüterjans, 1996; Prompers et al., 1998). More recently we presented 'out-and-back' type pulse sequences which link $^{1}H^{\varepsilon 1}/^{15}N^{\varepsilon 1}$ and $^{1}H^{\delta 2}/^{13}C^{\delta 2}$ with $^{13}C^{\beta}$ resonances in tryptophan and histidine side chains, respectively (Löhr et al., 2002). Owing to the use of [$^{15}N$, $^{1}H$]-TROSY (Pervushin et al., 1997) and/or [$^{13}C$, $^{1}H$]-TROSY (Pervushin et al., 1998; Brutscher et al., 1998) they could be successfully applied to proteins of up to 35 kDa molecular weight.

A common feature of the above mentioned experiments is that they rely on correlations with β-carbons and/or β-protons. If their resonance frequencies are unknown or degenerate, the sequence-specific assignment of aromatic resonances fails. Again focusing on tryptophan and histidine side chains we now introduce a three-dimensional pulse sequence which provides connectivities between δ-carbons or δ-protons and backbone NH groups of the sequentially following residues. Experimental parameters can be adjusted to detect either of the residue types in separate spectra or simultaneously in a single spectrum. Its application at the early stages of the sequential backbone assignment process yields valuable additional information which is analogous to that obtained in 2D amino acid type-selective $^{1}H$–$^{15}N$ correlation experiments (Schubert et al., 1999, 2001a, b).

Unambiguous assignments of tryptophan and histidine ring protons and protonated carbons beyond the δ-position require complementary experiments. Histidine $^{1}H^{\delta 2}/^{13}C^{\delta 2}$ and $^{1}H^{\varepsilon 1}/^{13}C^{\varepsilon 1}$ resonances belonging to the same imidazole ring can be identified using a combination of long-range $^{1}H$–$^{15}N$ (Bax et al., 1988; Schmidt et al., 1991; Pelton et al., 1993) and direct $^{1}H$–$^{13}C$ correlations. Equivalent information is available from a HCN triple-resonance experiment (Sudmeier et al., 1996) when it is recorded as a three-dimensional version. Here we describe a related method to correlate $^{1}H^{\delta 2}/^{13}C^{\delta 2}$ and $^{1}H^{\varepsilon 1}/^{13}C^{\varepsilon 1}$ chemical shifts in a single 2D experiment. The indole moiety of tryptophan side chains consists of two proton spin systems separated by the quarternary γ-, δ2- and ε2-carbons (see Figure 1 for the numbering scheme). Therefore, homonuclear $^{1}H$–$^{1}H$ or $^{1}H$–TOCSY-relayed $^{1}H$–$^{13}C$ correlation (Zerbe et al., 1996) experiments are able to provide connectivities within the six-membered ring, but the link to sequence-specifically assigned $^{1}H^{\delta 1}/^{13}C^{\delta 1}$ requires transfer of magnetization via $^{13}C$–$^{13}C$ isotropic mixing using experiments such as CCH–TOCSY (Fesik et al., 1990; Prompers et al., 1997), HCCH-TOCSY (Bax et al., 1990b) or (HC)C–(C)CH–TOCSY (Löhr and Rüterjans, 1996). While unambiguous results can often be obtained owing to the distinct aromatic $^{13}C$ chemical shifts of this residue type, the presence of several tryptophan residues in the protein may cause problems because of the rather low chemical shift dispersion at specific positions. In addition, signal overlap with other aromatic residue types is possible,

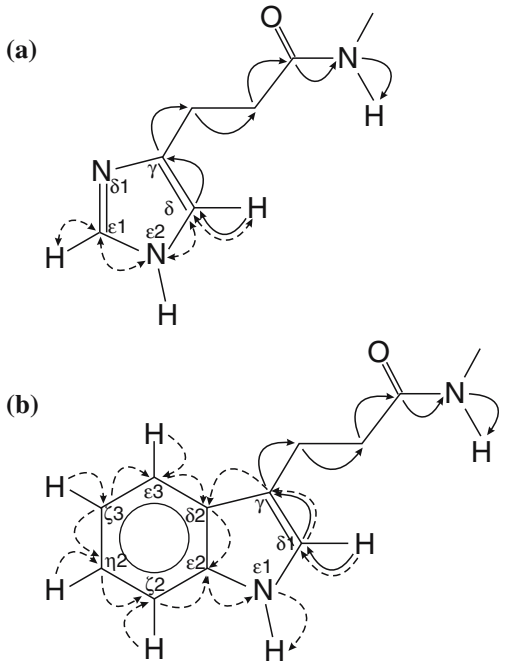


*Figure 1.* Graphical representation of magnetization transfer pathways in (a) histidine and (b) tryptophan side chains induced by the pulse sequences proposed in this paper. For clarity, atom identifiers of imidazole and indole ring systems have been included. The imidazole moiety of histidine is shown in the more abundant tautomeric state of the neutral form. Solid arrows represent an experiment for the sequence-specific assignment of δ-CH groups in both residue types. Connectivities between the latter and the remaining ring protons and directly bound carbons (and nitrogens in the case of tryptophan) are obtained as indicated by broken arrows.

complicating analysis of such spectra. To separate aromatic spin systems from individual tryptophan side chains and select against those of other amino acids it is proposed here to take advantage of the generally well dispersed indole $^{1}H$–$^{15}N$ resonances.

## Materials and methods

### *Description of the pulse sequences*

The flow of magnetization in each of the three novel experiments is outlined in Figure 1. For both histidine and tryptophan residues, the pulse sequence shown in Figure 2 affords direct correlations between their δ-protons/carbons and amide groups of the sequentially following amino acid. It exclusively employs one-bond scalar couplings to transfer magnetization in a 'straight-through' manner along the pathway $^{1}H_i^{\delta}(t_1) \rightarrow {}^{13}C_i^{\delta}(t_1) \rightarrow {}^{13}C_i^{\gamma} \rightarrow {}^{13}C_i^{\beta} \rightarrow {}^{13}C_i^{\alpha} \rightarrow {}^{13}C_i' \rightarrow {}^{15}N_{i+1}'(t_2) \rightarrow {}^{1}H_{i+1}^{N}(t_3)$ where δ refers to the δ2 and δ1 postions in histidine and tryptophan residues, respectively, and $i$ is their number in the amino acid sequence. Depending on whether $^{1}H^{\delta}$ or $^{13}C^{\delta}$ chemical shift evolution is monitored in $t_1$, the experiment is referred to as H(CDCGCBCACO)NH or (H)CD(CGCBCACO)NH. The initial INEPT (Morris and Freeman, 1979) sequence is followed by four concatenated CC–COSY elements that are either 'homonuclear' ($^{13}C^{\delta} \rightarrow {}^{13}C^{\gamma}$, $^{13}C^{\beta} \rightarrow {}^{13}C^{\alpha}$) or 'heteronuclear' ($^{13}C^{\gamma} \rightarrow {}^{13}C^{\beta}$, $^{13}C^{\alpha} \rightarrow {}^{13}C'$) in nature, the latter using separate semi-selective pulses for the two types of carbons involved. Delay settings for the $^{13}C^{\delta} \rightarrow {}^{13}C^{\gamma}$ transfer allow for a discrimination between individual aromatic amino acid types based on their spin topologies and differential $^{1}J_{C\delta C\gamma}$ coupling constants. Correlations for phenylalanine and tyrosine residues are not observed in HCD(CGCBCACO)NH experiments because (1) their δ-carbons have two homonuclear coupling partners as opposed to only one in histidine and tryptophan residues and (2) values of $^{1}J_{C\delta C\gamma}$ in the phenyl rings are 15–20 Hz lower than $^{1}J_{C\delta 2C\gamma}$ of imidazole and $^{1}J_{C\delta 1C\gamma}$ of indole rings (70–75 Hz). As a consequence, in periods $T_C$ ((H)CD(CGCBCACO)NH version) or η (H(CDCGCBCACO)NH version) adjusted to $\approx 1/(2\,{}^{1}J_{C\delta 2C\gamma})$ (His) $\approx 1/(2\,{}^{1}J_{C\delta 1C\gamma})$ (Trp) a large fraction of phenylalanine and tyrosine $^{13}C^{\delta}$ magnetization is dephased due to passive couplings with $^{13}C^{\varepsilon}$ spins and becomes inaccessible for the desired transfer pathway. In the subsequent ζ period of $\approx 3/(2\,{}^{1}J_{C\delta 2C\gamma})$ (His) $\approx 3/(2\,{}^{1}J_{C\delta 1C\gamma})$ (Trp) $\approx 1/{}^{1}J_{C\delta 2C\gamma}$ (Trp) $\approx 1/{}^{1}J_{C\delta 2C\gamma}$ (Phe, Tyr) rephasing of $^{13}C^{\gamma}$ magnetization with respect to the active $^{1}J_{C\delta C\gamma}$ couplings occurs for histidine and tryptophan but not for phenylalanine and tyrosine residues. Note that the passive $^{1}J_{C\delta 2C\gamma}$ coupling in tryptophan is not larger than one-bond $^{13}C$–$^{13}C$ couplings in phenyl rings, i.e. about 55 Hz.

Cross peaks of histidine and tryptophan residues in HCD(CGCBCACO)NH spectra can be distinguished from each other by their different signs resulting from the $\cos(\pi\,{}^{1}J_{C\delta 2C\gamma}\zeta) \approx -1$ factor introduced in the coherence transfer pathway of tryptophan by the δ2-carbon spin. Alternatively, separate experiments can be recorded for the two amino acid types. Setting ζ to a shorter value,

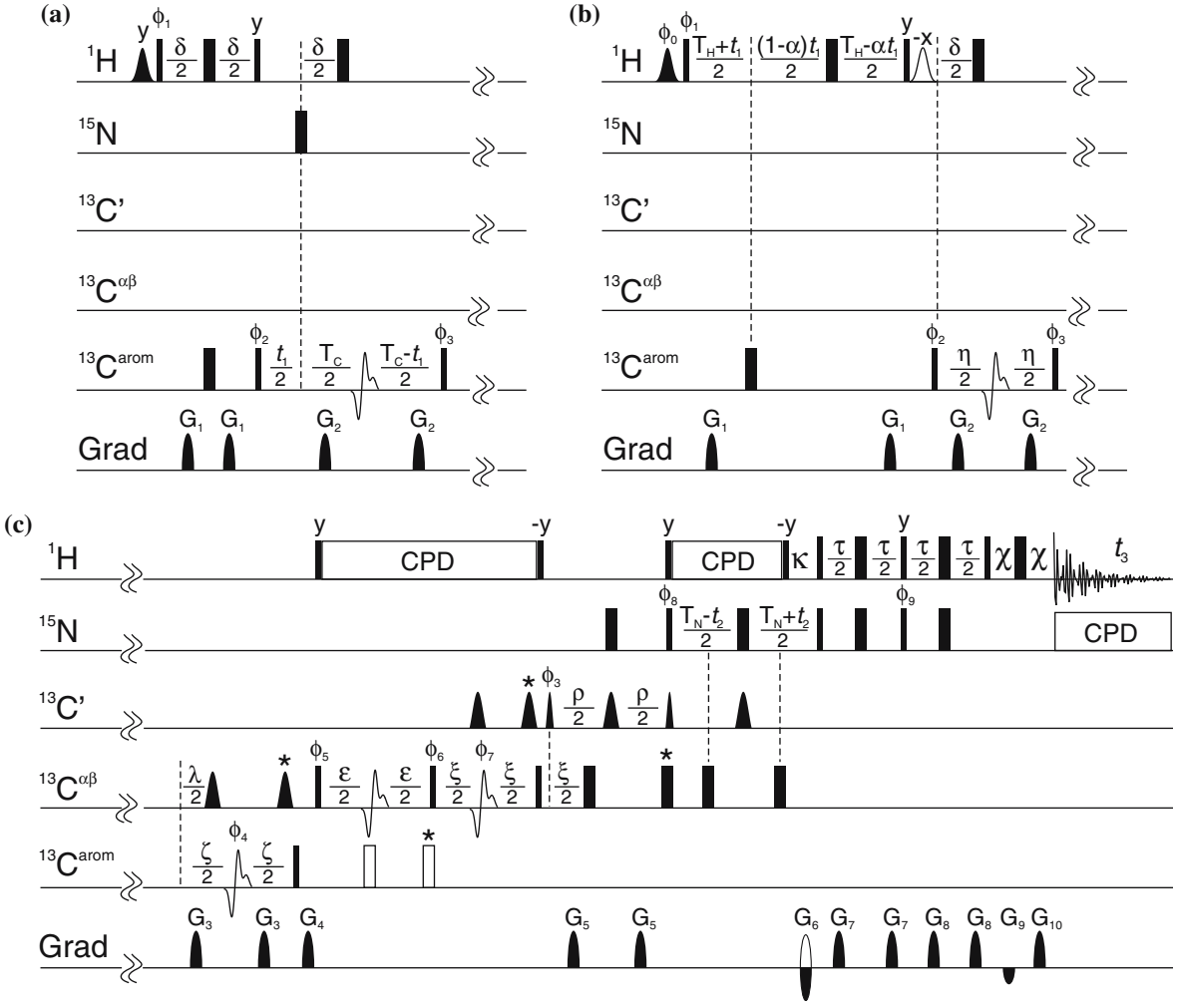


between $1/(2\,{}^1J_{C\delta 2C\gamma})$ (His) and $1/(2\,{}^1J_{C\delta 2C\gamma})$ (Trp), results in selective detection of histidine residues due to an almost complete dephasing of tryptophan $^{13}C^{\gamma}$ magnetization caused by the passive ${}^1J_{C\delta 2C\gamma}$ interaction. The reverse selection employs bandselective inversion pulses, relying on the fact that γ-carbons of tryptophan resonate approximately 20 ppm upfield from those of other aromatic side chains (Schubert et al., 2001b). A fraction $\lambda$ ($\leq 1/(2\,{}^1J_{C\gamma C\beta})$) of the ζ delay is used for the build up of $^{13}C^{\gamma}$ antiphase coherence with respect to $^{13}C^{\beta}$ which is converted to $^{13}C^{\beta}$ antiphase coherence by the following pair of 90° pulses. The latter magnetization term is refocussed during ε while simultaneously defocussing occurs with respect to $^{13}C^{\alpha}$. The remaining coherence transfer steps correspond to that of the CBCA(CO)NH experiment (Grzesiek and Bax, 1992) implemented with sensitivity enhancement and gradient coherence selection in the standard manner (Kay et al., 1992; Muhandiram and Kay, 1994). For further details of the pulse sequence including the handling of the water magnetization see the figure legend.

An experimental scheme to provide $^1H^{\delta 2}/^{13}C^{\varepsilon 1}$ and $^1H^{\varepsilon 1}/^{13}C^{\delta 2}$ correlations within histidine side chains is depicted in Figure 3. The two-dimensional pulse sequence, designated as (H)C(NC)H$^{His}$, is derived from the HCNCH technique (Sklenář et al., 1993a), developed to transfer magnetization from ribose H1′ to base H6 or H8 protons in RNA oligonucleotides via the intervening $^{13}C$ and $^{15}N$ nuclei, and also related to HCN experiment (Sudmeier et al., 1996), which links the two imidazole CH of histidine via common correlations to

*Figure 2.* Experimental schemes for correlating δ-carbons (version a, (H)CDCGCBCACO)NH) or δ-protons (version b, H(CDCGCBCACO)NH) of histidine and/or tryptophan residues with seqentially following backbone amides. Sequence c is appended to either of the two versions. Narrow and wide filled bars denote rectangular 90° and 180° pulses, respectively, applied with the highest available power for protons and nitrogens with carrier frequencies positioned at the water resonance ($^1$H) and the center of the amide region ($^{15}$N) throughout the sequences. Pulse widths given in the following are suitable for application at 600 MHz $^1$H frequency. Proton composite pulse decoupling (CPD) is applied along the x-axis and employs a DIPSI-2 sequence (Shaka et al., 1988) at an RF field strength of 5 kHz while $^{15}$N decoupling is achieved by GARP-1 modulation (Shaka et al., 1985) with a 0.8-kHz RF field. Gaussian shaped (truncation level 10%) 90° pulses of 2 ms duration ensure alignment of the water magnetization along the positive z axis at the start of acquisition (Grzesiek and Bax, 1993a; Stonehouse et al., 1994; Matsuo et al., 1996). For this purpose the phase of the first water-selective pulse ($\phi_0$) in version b is $y$ when the phase of the first unselective pulse ($\phi_1$) is $x$ or $-x$ and the second water-selective pulse (indicated by on open shape) is omitted. When $\phi_1$ becomes $y$ or $-y$, the latter pulse is applied and $\phi_0$ must be changed to $x$. The carbon carrier frequency is placed at 123 ppm (center of $^{13}C^{\gamma}/^{13}C^{\delta}$ resonance region of His and Trp residues) at the beginning of the sequence. The initial hard 180° $^{13}$C pulse is applied with an RF field of about 8 kHz. For the following four rectangular 90° pulses the RF field is reduced to $\Delta/\sqrt{15}$, where δ is the difference (in Hz) between 123 ppm and the centre of the His/Trp $^{13}C^{\beta}$ spectral region (ca. 30 ppm) and the carrier frequency is jumped to 30 ppm between the third and fourth 90° pulse. The next two 90° pulses (flanking the ξ period) are applied at 42 ppm (between His/Trp $^{13}C^{\beta}$ and $^{13}C^{\alpha}$ chemical shifts) using phase modulation (Boyd and Soffe, 1989; Patt, 1992) and employ an RF field of $\delta/\sqrt{15}$, where δ is recalculated to match the difference between this offset and the centre of the carbonyl region (≈176 ppm). Band-selective refocussing in the centre of the $T_C$ (version a) or η (version b), ζ, ε and ξ periods is achieved by G$^3$ Gaussian cascades (Emsley and Bodenhausen, 1990) with a duration of 300 μs, where the first and second are applied at 123 ppm and the third and fourth at 42 ppm. Phase modulated 180° pulses on β-carbon during ζ have the shape of the centre lobe of a $\sin(x)/x$ function and a width of 120 μs. The same shape and duration is used for 90° and 180° pulses on $^{13}C'$ applied at 176 ppm. The last four rectangular pulses are applied at 56 ppm to invert $^{13}C^{\alpha}$ magnetization with an RF field strength of $\Delta/\sqrt{3}$, Δ denoting the difference between the $^{13}C^{\alpha}$ and the carbonyl region. Pulses labelled with an asterisk are inserted to compensate Bloch–Siegert-like phase shifts. Depending on whether correlations should be observed for histidine or tryptophan residues or both, the duration and offset of 180° pulses on aromatic carbons during ε (indicated by open rectangles) as well as the duration of periods ζ and λ are varied: A His-selective version is obtained using 100-μs sinc-shaped pulses applied at 132 ppm and $\zeta = \lambda = 7.8$ ms, which is a compromise between $1/(2\,{}^1J_{C\delta2C\gamma})$ in histidine (≈ 6.6 ms) and $1/(2\,{}^1J_{C\delta2C\gamma})$ in tryptophan (≈ 9 ms). Note that ${}^1J_{C\delta2C\gamma}$ is the active coupling in the former and a passive coupling in the latter case. Extending the pulse width to 300 μs while shifting its offset to 111 ppm and adjusting ζ and λ to 19 ms ($\approx 3/(2\,{}^1J_{C\delta1C\gamma}) \approx 1/{}^1J_{C\delta2C\gamma}$) and 11 ms ($\approx 1/(2\,{}^1J_{C\gamma C\beta})$), respectively, is required for the Trp-selective version. Both amino acid types are detected when these delay settings are retained but a rectangular 180° pulse is applied at 123 ppm with an RF field of $\Delta/\sqrt{3}$, where Δ is the difference (in Hz) between 123 and 30 ppm. In all cases further delays are adjusted as follows: $\delta = T_H = 2.6$ ms ($\approx 1/(2\,{}^1J_{H\delta C\delta})$); $\eta = T_C = 6.4$ ms ($\leq 1/(2\,{}^1J_{C\delta2C\gamma})$ (His)$\approx 1/(2\,{}^1J_{C\delta1C\gamma})$ (Trp)); $\varepsilon = 9.6$ ms ($\leq 1/(2\,{}^1J_{C\gamma C\beta})$); $\xi = 9.2$ ms ($\approx 1/(2\,{}^1J_{C\alpha C'})$); $\rho = 21$ ms ($\leq 1/(2\,{}^1J_{C'N})$); $T_N = 24$ ms ($\leq 1/(2\,{}^1J_{C'N})$); $\kappa = 5.4$ ms ($\approx 1/(2\,{}^1J_{NH})$); $\tau = 4.5$ ms ($\leq 1/(2\,{}^1J_{NH})$); $\chi = 0.38$ ms (duration of $G_9$ and $G_{10}$ + recovery time). In version b, $t_1$ is a semi-constant time evolution period (Logan et al., 1992; Grzesiek and Bax, 1993b), where the parameter α is defined by $T_H/t_{1max}$. Unless specified, pulses are applied along the $x$-axis. Phase cycling is: $\phi_1 = 4(x), 4(-x)$; $\phi_2 = x, -x$; $\phi_3 = 8(x), 8(-x)$; $\phi_4 = 32(x), 32(y)$; $\phi_5 = 2(x), 2(-x)$; $\phi_6 = 4(x), 4(-x)$; $\phi_7 = 16(x), 16(y)$; $\phi_8 = x$; $\phi_9 =$ y; reveiver = R, 2(−R), R, −R, 2(R), −R, where R = $x$, 2(−$x$), $x$, −$x$, 2($x$), −$x$. Quadrature in $t_1$ is achieved by altering $\phi_2$ (version a) or $\phi_1$ (version b) in the States-TPPI (Marion et al., 1989) manner. Gradients are sine-bell shaped and have the following durations, peak amplitudes and directions: $G_1$ = (0.15 ms, 7.5 G/cm, $x$), $G_2$ = (0.15 ms, 7.5 G/cm, $y$), $G_3$ = (0.5 ms, 6 G/cm, $x$), $G_4$ = (0.5 ms, 5 G/cm, $y$), $G_5$ = (0.5 ms, 7.5 G/cm, $x$), $G_6$ = (1.4 ms, −19.73 G/cm, $xyz$), $G_7$ = (0.3 ms, 4 G/cm, $xy$), $G_8$ = (0.3 ms, 5.5 G/cm, $xy$), $G_9$ = (0.175 ms, −2.5 G/cm, $xyz$), $G_{10}$ = (0.175 ms, 13.5 G/cm, $xyz$). For each $t_2$ increment echo- and antiecho coherence transfer pathways are selected alternately by inversion of the polarity of $G_6$ along with the pulse phase $\phi_9$ and spectra are processed using the enhanced sensitivity method (Cavanagh et al., 1991; Kay et al., 1992). Axial peaks in the $^{15}$N dimension are shifted to the edge of the spectrum by incrementing $\phi_8$ and the receiver phase by 180° for each successive value of $t_2$.

nitrogen chemical shifts detected in a third dimension. While the HCN sequence is of the 'out-and-back' type and the HCNCH exclusively transfers magnetization in a 'straight through' manner, the experiment proposed here allows for both pathways. As the major difference with respect to the original HCNCH sequence, source and destination CH groups are treated as 'like' spins in the (H)C(NC)H$^{His}$ experiment, rendering the magnetization transfer bidirectional and giving rise to additional $^1H^{\delta2}/^{13}C^{\delta2}$ or $^1H^{\varepsilon1}/^{13}C^{\varepsilon1}$ auto-correlation peaks by retaining magnetization not relayed between the two carbon sites via $^{13}C$–$^{15}N$ scalar couplings.

Neglecting relaxation as well as the $^1H$–$^{13}C$ INEPT and reverse INEPT steps, intensities of $(\omega_1/\omega_2)$ $^{13}C^{\delta2}/^1H^{\varepsilon1}$ ($I_1$), $^{13}C^{\varepsilon1}/^1H^{\delta2}$ ($I_2$), $^{13}C^{\delta2}/^1H^{\delta2}$ ($I_3$) and $^{13}C^{\varepsilon1}/^1H^{\varepsilon1}$ ($I_4$) signals in the (H)C(NC)H$^{His}$ are proportional to:

$$\begin{aligned}&\sin(\pi\,{}^1J_{C_{\delta2}N_{\varepsilon2}}T_C)\cos(\pi\,{}^2J_{C_{\delta2}N_{\delta1}}T_C)\\&\cos(\pi\,{}^1J_{C_{\delta2}C_{\gamma}}T_C)\ \sin(\pi\,{}^1J_{C_{\delta2}N_{\varepsilon2}}\varepsilon)\ \sin(\pi\,{}^1J_{C_{\varepsilon1}N_{\varepsilon2}}\varepsilon)\\&\sin(\pi\,{}^1J_{C_{\varepsilon1}N_{\varepsilon2}}\zeta)\ \cos(\pi\,{}^1J_{C_{\varepsilon1}N_{\delta1}}\zeta)\end{aligned}\qquad (I_1)$$

$$\begin{aligned}&\sin(\pi\,{}^1J_{C_{\varepsilon1}N_{\varepsilon2}}T_C)\ \cos(\pi\,{}^1J_{C_{\varepsilon1}N_{\delta1}}T_C)\\&\sin(\pi\,{}^1J_{C_{\varepsilon1}N_{\varepsilon2}}\varepsilon)\ \sin(\pi\,{}^1J_{C_{\delta2}N_{\varepsilon2}}\varepsilon)\ \sin(\pi\,{}^1J_{C_{\delta2}N_{\varepsilon2}}\zeta)\\&\cos(\pi\,{}^2J_{C_{\delta2}N_{\delta1}}\zeta)\ \cos(\pi\,{}^1J_{C_{\delta2}C_{\gamma}}\zeta)\end{aligned}\qquad (I_2)$$

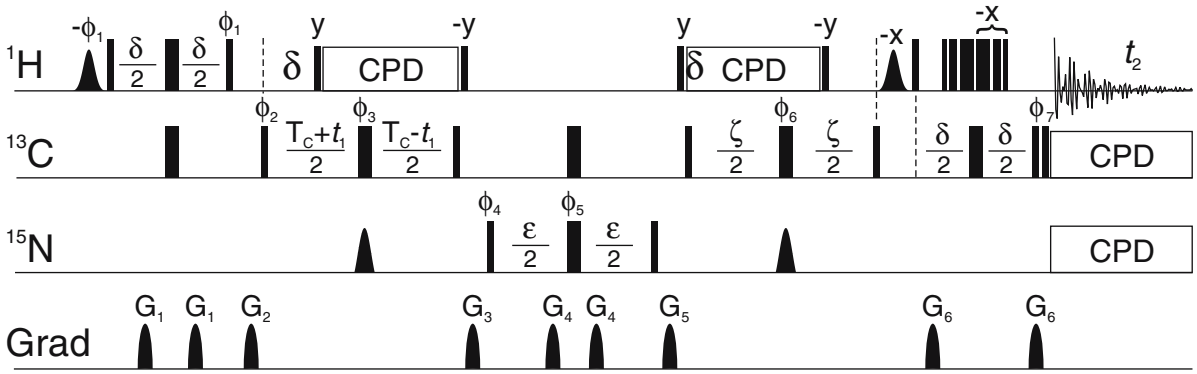


*Figure 3.* Pulse sequence of the 2D (H)C(NC)H$^{His}$ experiment for the correlation of $^1H^{\delta2}/^{13}C^{\delta2}$ with $^1H^{\varepsilon1}/^{13}C^{\varepsilon1}$ chemical shifts in histidine side chains. Proton, carbon and nitrogen carrier frequencies are centered at the water (≈4.75 ppm), the aromatic region (128 ppm) and the region of imidazole NH groups (≈170 ppm), respectively. Rectangular pulses on $^1$H and $^{15}$N are applied with the highest available power, while pulses on $^{13}$C employ a 10 kHz RF field. Solvent suppression is achieved with Gaussian-shaped $^1$H flip-back pulses of 2.5 ms length in combination with the 3-9-19 selective hard-pulse (Sklenář et al., 1993b) based WATERGATE (Piotto et al., 1992) in the reverse INEPT step. RF field strength for $^1$H (DIPSI-2), $^{13}$C (GARP-1) and $^{15}$N (GARP-1) CPD are 4.2, 2.1 and 0.5 kHz, respectively. A 1-ms i-SNOB-2 (Kupče et al., 1995) pulse is used for selective inversion of protonated imidazole nitrogens during periods $T_C$ and ζ. Delay durations are δ = 2.5 ms (≈ $1/(2^1J_{HC\delta2/\varepsilon1})$); $T_C = \zeta = 14$ ms (≈ $1/^1J_{C\delta2C\gamma}$); ε = 16–18 ms (≤ $1/(4^1J_{C\delta2/\varepsilon1N\varepsilon2})$. The default pulse phase is $x$. Other pulse phases are cycled according to: $\phi_1 = 4(y), 4(-y)$; $\phi_2 = x$; $\phi_3 = x, y$; $\phi_4 = 2(x), 2(-x)$; $\phi_5 = 8(x), 8(y)$; $\phi_6 = 16(x), 16(y)$; $\phi_7 = x, -x$; reveiver = $R, 2(-R), R$ with $R = x, 2(-x), x, -x, 2(x), -x$. Sign discrimination in the $t_1$ dimension is accomplished by States-TPPI of $\phi_2$. Durations, peak amplitudes and directions of pulsed field gradients are: $G_1$ = (0.5 ms, 5 G/cm, $x$), $G_2$ = (0.5 ms, 5 G/cm, $y$), $G_3$ = (0.5 ms, 7.5 G/cm, $x$), $G_4$ = (0.5 ms, 7.5 G/cm, $y$), $G_5$ = (0.5 ms, 6 G/cm, $x$), $G_6$ = (0.3 ms, 35 G/cm, $xyz$).

$$\begin{aligned}
&\sin(\pi\,{}^1J_{C_{\delta2}N_{\varepsilon2}}T_C)\ \cos(\pi\,{}^2J_{C_{\delta2}N_{\delta1}}T_C)\\
&\cos(\pi\,{}^1J_{C_{\delta2}C_\gamma}T_C)\ \cos(\pi\,{}^1J_{C_{\delta2}N_{\varepsilon2}}\varepsilon)\\
&\cos(\pi\,{}^1J_{C_{\varepsilon1}N_{\varepsilon2}}\varepsilon)\ \sin(\pi\,{}^1J_{C_{\delta2}N_{\varepsilon2}}\zeta)\\
&\cos(\pi\,{}^2J_{C_{\delta2}N_{\delta1}}\zeta)\ \cos(\pi\,{}^1J_{C_{\delta2}C_\gamma}\zeta)
\end{aligned}\qquad (I_3)$$

$$\begin{aligned}
&\sin(\pi\,{}^1J_{C_{\varepsilon1}N_{\varepsilon2}}T_C)\ \cos(\pi\,{}^1J_{C_{\varepsilon1}N_{\delta1}}T_C)\\
&\cos(\pi\,{}^1J_{C_{\varepsilon1}N_{\varepsilon2}}\varepsilon)\ \cos(\pi\,{}^1J_{C_{\delta2}N_{\varepsilon2}}\varepsilon)\\
&\sin(\pi\,{}^1J_{C_{\varepsilon1}N_{\varepsilon2}}\zeta)\ \cos(\pi\,{}^1J_{C_{\varepsilon1}N_{\delta1}}\zeta)+\\
&\sin(\pi\,{}^1J_{C_{\varepsilon1}N_{\delta1}}T_C)\cos(\pi\,{}^1J_{C_{\varepsilon1}N_{\varepsilon2}}T_C)\\
&\cos(\pi\,{}^1J_{C_{\varepsilon1}N_{\delta1}}\varepsilon)\ \cos(\pi\,{}^1J_{C_\gamma N_{\delta1}}\varepsilon)\\
&\cos(\pi\,{}^2J_{C_{\delta2}N_{\delta1}}\varepsilon)\ \sin(\pi\,{}^1J_{C_{\varepsilon1}N_{\delta1}}\zeta)\\
&\cos(\pi\,{}^1J_{C_{\varepsilon2}N_{\varepsilon2}}\zeta)
\end{aligned}\qquad (I_4)$$

where only one-bond $^{13}$C–$^{15}$N couplings are considered for coherence transfer. It should be noted that the magnitude of individual $^1J_{CN}$ and $^2J_{CN}$ coupling constants is strongly dependent on the protonation and tautomeric state of the imidazole ring system (Blomberg et al., 1977; Alei Jr., 1980; Sudmeier et al., 1996; Shimba et al., 1998, 2003). In general, $^1J$ couplings involving protonated nitrogens are large (≥11 Hz) whereas those involving unprotonated nitrogens are smaller by about an order of magnitude and $^2J_{C_{\delta2}N_{\delta1}}$ is only observable (≈5 Hz) for the $N^{\delta1}$–H tautomer. Therefore in the cationic state and the $N^{\varepsilon2}$–H tautomeric state of uncharged histidine, magnetization can exclusively be transferred via the ε2-nitrogen as is assumed in the above expressions. This pathway is however precluded in the $N^{\delta1}$–H tautomeric state and the alternative transfer via $^1J_{C_{\varepsilon1}N_{\delta1}}$ and $^2J_{C_{\delta2}N_{\delta1}}$ is very inefficient because of the small size of the latter coupling in the presence of a large passive $^1J_{C_\gamma N_{\delta1}}$ interaction. Attenuation of signal amplitudes due to the evolution of the $^1J_{C_{\delta2}C_\gamma}$ coupling during the de- and refocussing of carbon magnetization with respect to nitrogens is avoided by adjusting delays $T_C$ and ζ to the inverse of the coupling constant. The relative intensity of cross peaks ($I_1$, $I_2$) and auto peaks ($I_3$, $I_4$) can be tuned by the setting of the $^{15}$N relay period ε. Both types can normally by detected using values of 16–18 ms, auto peaks being somewhat more intense. The band-selective 180° $^{15}$N pulses applied during these periods ensure that magnetization is exclusively transferred to and from protonated imidazole nitrogens. They may be replaced by non-selective pulses without significant loss due to passive couplings involving unprotonated nitrogens, which resonate at lower field, but then

$^{1}H^{\delta1}/^{13}C^{\delta1}$ autocorrelation peaks of tryptophan residues will be observed, too.

Figure 4 shows a four-dimensional pulse sequence for correlating tryptophan $^{1}H^{\varepsilon1}/^{15}N^{\varepsilon1}$ chemical shifts with those of all aromatic $^{1}H$–$^{13}C$ groups in the same ring system. It represents a simple adaptation of the HC(C)NH–TOCSY experiment (Logan et al., 1992; Lyons and Montelione, 1993), normally employed to link side-chain protons and/or carbons to backbone amides, to the indole spin system. After the initial refocused INEPT, comprising $^{1}H$ ($t_1$) and $^{13}C$ ($t_2$) chemical shift labelling, in-phase carbon magnetization is relayed along the $^{13}C$–$^{13}C$ scalar coupling network via isotropic mixing. It was found empirically that a spin-lock time of 10 ms yields relatively uniform intensities for all ring positions. The destination carbon spin in the HC(C)NH–TOCSY$^{Trp}$ experiment is $^{13}C^{\varepsilon2}$ instead of $^{13}C^{\alpha}$ as in the original version. Its unique resonance frequency ($139 \pm 1$ ppm) which is well-separated from the remaining aromatic carbons in tryptophan side chains allows for selective refocusing and inversion, respectively, in the subsequent $\Delta$ and $T_N$ periods during which the polarization transfer to the adjacent ε1-nitrogen takes place. Thus, interference from passive couplings such as $^{1}J_{C_{\varepsilon2}C_{\zeta2}}$, $^{1}J_{C_{\varepsilon2}C_{\delta2}}$ and $^{1}J_{C_{\delta1}N_{\varepsilon1}}$ is eliminated (except for the latter coupling in the four-dimensional version) and the optimal durations of $\delta$ and $T_N$ ($\leq 1/(2\,^{1}J_{C_{\varepsilon2}N_{\varepsilon1}})$) are only compromised by transverse relaxation. On the other hand, this renders the direct $^{13}C^{\delta1} \rightarrow {}^{15}N^{\varepsilon1}$ transfer impossible. Recording of $^{1}H^{\delta1}/^{13}C^{\delta1}$ chemical shifts which is crucial for the sequence-specific assignment of the remaining indole resonances requires a 'diversion' of $^{13}C^{\delta1}$ magnetization via the non-protonated γ-, δ2- and ε2-carbons. Selection of the alternative pathway $^{1}H(t_1) \rightarrow {}^{13}C(t_2)$ CC–TOCSY $\rightarrow$ $^{13}C^{\delta1} \rightarrow {}^{15}N^{\varepsilon1}(t_3) \rightarrow {}^{1}H^{\varepsilon1}(t_4)$ would suffer from the smaller $^{1}J_{C_{\delta1}N_{\varepsilon1}}$ coupling constant compared to $^{1}J_{C_{\varepsilon2}N_{\varepsilon1}}$ and the longer CC–TOCSY mixing time required to allow for the larger number of transfer steps from $^{13}C^{\zeta2}$, $^{13}C^{\zeta3}$ and $^{13}C^{\eta2}$.

*Sample preparations*

The preparation of [$U$–$^{13}C$;$^{15}N$]-enriched RNase T1 has been described elsewhere (Spitzner et al., 2001). The sample for NMR measurements had a protein concentration of 2 mM in a volume of 500 µl containing 90% $H_2O$ and 10% $D_2O$ with the pH adjusted to 5.5.

Recombinant family 11 xylanase from *Bacillus agaradhaerens* was expressed in *E. coli* carrying the pET-3a plasmid, encoding for residues 1–207. Uniform $^{13}C/^{15}N$ labelling was achieved by growing cells on M9 minimal medium supplemented with 1 g/l $^{13}C_6$ glucose, 2.5 g/l $^{13}C_3$ glycerol and 1 g/l $^{15}NH_4Cl$. Protein purification followed the procedure of Sabini et al. (1999). The sample was dissolved at a concentration of 1.3 mM in 10 mM sodium acetate buffer, pH 5.4, containing 0.03% $NaN_3$ and 50 µg/ml Pefabloc protease inhibitor.

The gene encoding a truncation (amino acids 1–120) of the human cell division cycle protein (hCdc5) was cloned into a pET11 vector which was then transformed into *E. coli* BL21(DE3). The bacteria were cultured overnight at 30 °C in LB medium and transferred to M9 medium containing 1 g/l $^{15}NH_4Cl$ and 2 g/l $^{13}C_6$ glucose. Seven hours after induction with IPTG cells were harvested by centrifugation and resuspended in 50 mM Tris·HCl (pH = 7.5) + 50 mM NaCl + 5 mM EDTA + 10 mM β-mercaptoethanol. Cells were disrupted using a French press. Purification of protein which contained a C-terminal $(His)_6$-tag, involved $Ni^{2+}$-NTA affinity and gel filtration chromotographies. The NMR sample contained 0.6 mM of the doubly labelled protein, dissolved in 20 mM sodium acetate buffer at pH 5.5, to which 10 mM β-mercaptoethanol had been added.

The isolation and purification of the C-terminal receiver domain of *E. coli* sensor kinase RcsC (RcsC-PR), containing the amino acids 684–933 and a C-terminal $(His)_6$-tag, was carried out according to an earlier published protocol (Rogov et al., 2004). Uniform $^{13}C/^{15}N$ labelling was achieved by growing the strain M15/pREP4/pQ-RcsC-PR in M9 medium containing 1 g/l $^{15}NH_4Cl$, 2 g/l $^{13}C_6$ glucose and 1 g/l $^{13}C_3$ glycerol. For NMR measurements the protein was equilibrated with 33 mM Tris–HCl buffer, pH 7.5, supplemented with 125 mM NaCl, 5 mM β-mercaptoethanol and 1 mM Tris-(2-carboxyethyl)-phosphine hydrochloride (TCEP–HCl) and concentrated to 0.8 mM by ultrafiltration.

Expression and purification of [$U$–$^{13}C$;$^{15}N$]-labelled flavodoxin from *Desulfovibrio vulgaris* was performed as described previously (Knauf et al.,

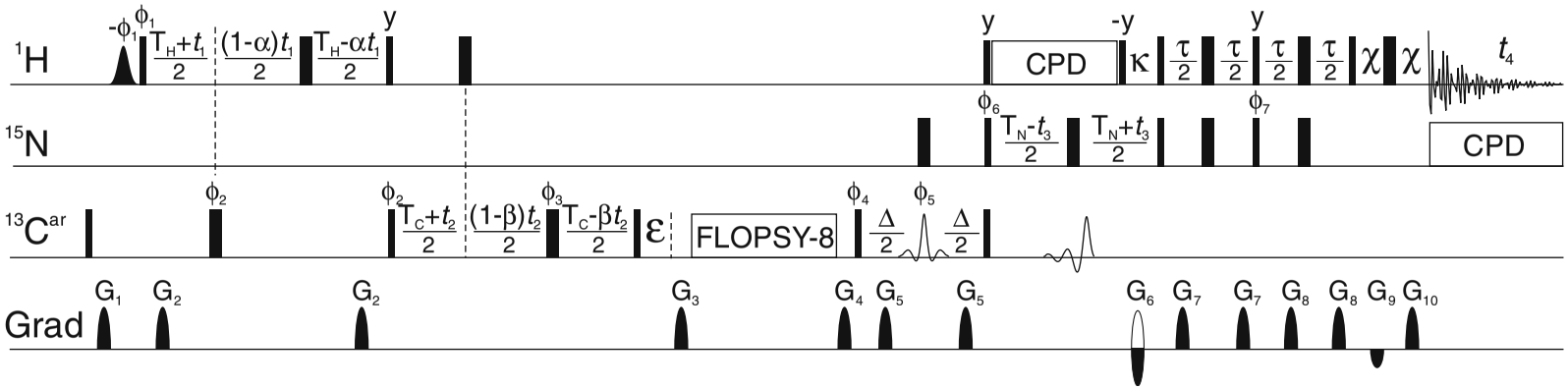


*Figure 4*. Four-dimensional HC(C)NH–TOCSY$^{Trp}$ pulse sequence for correlating $^1$H and $^{13}$C resonances of indole ring CH groups with $^1H^{\varepsilon 1}/^{15}N^{\varepsilon 1}$ resonances in tryptophan side chains. Rectangular $^1$H, $^{13}$C and $^{15}$N pulses, $^1$H (DIPSI-2) and $^{15}$N (GARP-1) CPD are applied with RF fields of approximately 29, 12, 6, 4.2 and 0.8 kHz, respectively. The initial Gaussian shaped 90° $^1$H pulse of 5 ms duration is applied at the water frequency while the offset for all other proton pulses is 6.7 ppm. In the first part of the sequence, the carbon carrier is placed at 121 ppm (center of protonated indole $^{13}$C chemical shifts), then set to 126.5 ppm (center of all indole $^{13}$C chemical shifts) during the CC–TOCSY transfer and finally switched to the $^{13}C^{\varepsilon 2}$ region (139 ppm). The nitrogen carrier frequency is 130 ppm throughout the sequence. Isotropic mixing of $^{13}$C magnetization is achieved with two cycles of FLOPSY-8 (Mohebbi and Shaka, 1991) at an RF field of 4.7 kHz, corresponding to a mixing time of 10 ms. Selective refocussing (during $\Delta$) and inversion (during $T_N$) of $^{13}C^{\varepsilon 2}$ magnetization is accomplished with 4-ms RE-BURP and 3-ms I-BURP-2 (Geen and Freeman, 1991) pulses, respectively (at 500 MHz $^1$H frequency). Delays $T_H = T_C$ ($\approx 1/(2^1J_{HC})$),$\Delta(\leq 1/(2^1J_{C_{\varepsilon 2}N_{\varepsilon 1}}))$, $T_N(\leq 1/(2^1J_{C_{\varepsilon 2}N_{\varepsilon 1}}))$, $\kappa(\approx 1/(2^1J_{NH}))$,$\tau(\leq 1/(2^1J_{NH}))$ and $\chi$ are adjusted to 2.6, 18, 25, 5.4, 4.5 and 0.38 ms, respectively. Here, $T_N$ includes the duration of the selective $^{13}$C 180° pulse whereas $\Delta$ does not. Evolution times $t_1$ and $t_2$ are of the semi-constant time type with $\alpha = T_H/t_{1max}$ and $\beta = T_C/t_{2max}$. Phase cycling: $\phi_1 = 16(x), 16(-x)$; $\phi_2 = y, -y$; $\phi_3 = 8(x), 8(-x)$; $\phi_4 = 2(y), 2(-y)$; $\phi_5 = 4(x), 4(y)$; $\phi_6 = 8(x), 8(-x)$; $\phi_7 = y$; reveiver $= R, 2(-R), R$ where $R = x, 2(-x), x, -x, 2(x), -x$. For each $t_3$ increment echo- and antiecho coherence transfer pathways are selected alternately by concerted inversion of $\phi_7$ and $G_6$. Axial peaks in the $^{15}$N dimension are shifted to the edge of the spectrum by incrementing $\phi_8$ and the receiver phase by 180° after each $t_3$ increment. States-TPPI is applied to $\phi_1$ and $\phi_2$, respectively, to obtain quadrature detection in the $t_1$ and $t_2$ dimensions. Note that the phase of the water-selective pulse is changed along with the phase of the first unselective 90° $^1$H pulse. As a result, irrespective of the setting of $\phi_1$ the water magnetization is aligned along $z$ before the second unselective 90° $^1$H pulse which rotates it to the transverse plane. The water magnetization is then brought back to the positive $z$ axis by constructive use of radiation damping (Jahnke and Kessler, 1994; Lippens et al., 1995; Otting and Liepinsh, 1995) which necessitates insertion of a delay $\varepsilon$ (20 ms with the instrumentation used) after $^{13}$C in-phase coherence is stored along the $z$ axis but before application of the next pulsed field gradient, $G_3$. The remaining proton pulses have no net effect on the water magnetization resulting in good solvent suppression and no saturation of exchanging $H^{N\varepsilon 1}$ spins for both real and imaginary parts of $t_1$ interferograms. Alternatively, if the proton carrier frequency is placed at the water resonance the method used in the H(CDCGCBCACO)NH pulse sequence (see Figure 2b) can be applied. Pulsed field gradients are applied with the following durations, peak amplitudes and directions: $G_1$ = (0.5 ms, 5 G/cm, $x$), $G_2$ = (0.15 ms, 10 G/cm, $y$), $G_3$ = (0.5 ms, 7.5 G/cm, $x$), $G_4$ = (0.5 ms, 6 G/cm, $y$), $G_5$ = (0.5 ms, 6.5 G/cm, $x$), $G_6$ = (1.4 ms, −19.73 G/cm, $xyz$), $G_7$ = (0.3 ms, 4 G/cm, $xy$), $G_8$ = (0.3 ms, 5.5 G/cm, $xy$), $G_9$ = (0.175 ms, −2.5 G/cm, $xyz$), $G_{10}$ = (0.175 ms, 13.5 G/cm, $xyz$).

1993), using M9 medium with $^{15}NH_4Cl$ as nitrogen source and $^{13}C_6$ glucose as well as $^{13}C_3$ glycerol as carbon sources. Measurements were carried out on the oxidized species of the protein, dissolved in 10 mM potassium phosphate buffer, pH 7.0. The solution contained 2.1 mM of the protein as well as 0.02% sodium azide, 50 μg/ml Pefabloc protease inhibitor and 0.3 mM EDTA.

After addition of 0.15 mM 3-(trimethylsilyl)-1-propanesulfonic acid (DSS) as internal chemical shift standard and 5% $D_2O$, xylanase, hCdc5, RcsC-PR and flavodoxin samples were placed in Shigemi microcells with total volumes ranging from 250 to 300 μl. Xylanase and flavodoxin samples were approximately four years old at the time when the measurements described here were performed. Thus, although both proteins are very stable, they contained small amounts of degradation products giving rise to sharp signals in some of the spectra shown at positions close to the respective random coil chemical shifts.

*Data acquisition and processing*

Experiments were performed at proton Larmor frequencies of 500 and 600 MHz on Bruker DMX, DRX or Avance spectrometers. A cryogenic $^1H\{^{13}C, ^{15}N\}$ triple resonance probe with *z*-gradient accessory was employed to record HCD(CGCBCACO)NH spectra of hCdc5 (note that in this case pulsed field gradients along *z* substituted for those along *x* and *y* directions, indicated in the legend of Figure 2). All remaining spectra were obtained with conventional 5-mm three-axis gradient $^1H\{^{13}C, ^{15}N\}$ triple resonance probes. Temperature settings were 29, 25, 23, 37 and 27 °C during experiments with xylanase, hCdc5, RcsC-PR, RNase T1 and flavodoxin, respectively.

Acquisition parameters of all two- and three-dimensional experiments carried out on each protein are listed in Table 1. In the H(CDCGCBCACO)NH experiments, spectral widths in the indirect proton dimension were chosen such that

*Table 1.* Acquisition parameters employed for recording two- and three-dimensional spectra shown in Figures 5–11

| Protein | Experiment | Frequency [MHz] | Spectral widths [ppm] | | | Time domain data[a] | | | Acquisition times [ms] | | | Scans/ FID | Exp. time [h] |
|---|---|---|---|---|---|---|---|---|---|---|---|---|---|
| | | | $F_1$ | $F_2$ | $F_3$ | $t_1$ | $t_2$ | $t_3$ | $t_1$ | $t_2$ | $t_3$ | | |
| Xylanase | 2D (HCDCGCBCACO)NH[b] | 600 | 32.1 | 13.5 | | 48 | 512 | | 13 | 63.3 | | 384 | 12 |
| | 3D H(CDCGCBCACO)NH | 600 | 2.5 | 30 | 13.5 | 24 | 36 | 512 | 15.3 | 19.2 | 63.3 | 64 | 69 |
| | 2D (H)C(NC)H$^{His}$ | 500 | 35.5 | 10 | | 60 | 384 | | 13.2 | 76.8 | | 256 | 9 |
| | 3D HC(CN)H–TOCSY$^{Trp}$ | 500 | 3.1 | 19 | 12 | 22 | 16 | 384 | 13.4 | 6.3 | 63.9 | 96 | 48 |
| hCdc5 | 2D TROSY-H(NCDCG)CB | 600 | 15.8 | 13 | | 20 | 512 | | 8.4 | 65.8 | | 1536 | 29.5 |
| | 3D H(CDCGCBCACO)NH | 600 | 3 | 27.8 | 10 | 28 | 40 | 320 | 15 | 23.1 | 53.3 | 64 | 96.5 |
| | 3D (H)CD(CGCBCACO)NH | 600 | 22.9 | 27.8 | 10 | 22 | 40 | 320 | 6.1 | 23.1 | 53.3 | 64 | 76 |
| RcsC-PR | 2D TROSY-H(CDCG)CB | 600 | 10.2 | 9 | | 18 | 512 | | 11 | 95.1 | | 64 | 1 |
| | 3D H(CDCGCBCACO)NH | 600 | 2.2 | 32.1 | 13.5 | 18 | 48 | 512 | 12.9 | 24 | 63.4 | 64 | 72 |
| | 3D (H)CD(CGCBCACO)NH | 600 | 20.7 | 32.1 | 13.5 | 20 | 48 | 512 | 6.1 | 24 | 63.4 | 64 | 84 |
| | 3D HC(CN)H–TOCSY$^{Trp}$ | 500 | 3.1 | 19 | 11 | 20 | 14 | 384 | 12.1 | 5.4 | 69.9 | 128 | 59 |
| RNase T1 | 2D H(CDCGCBCACON)H | 500 | 2.8 | 12 | | 24 | 512 | | 16.4 | 85.2 | | 64 | 1 |
| | 2D (H)C(NC)H$^{His}$ | 500 | 36.1 | 10 | | 60 | 256 | | 13 | 51.2 | | 64 | 1.75 |
| | 3D HC(CN)H–TOCSY$^{Trp}$ [c] | 500 | 2 | 17 | 7 | 16 | 14 | 256 | 15 | 6.1 | 73.1 | 16 | 4 |
| Flavodoxin | 2D (H)CD(CGCBCACON)H | 500 | 19.9 | 12 | | 16 | 512 | | 6 | 85.2 | | 64 | 0.75 |
| | 2D (H)C(NC)H$^{His}$ | 500 | 36.1 | 10 | | 64 | 384 | | 13.9 | 76.8 | | 32 | 1 |
| | 3D HC(CN)H–TOCSY$^{Trp}$ [c] | 500 | 2.5 | 17 | 11 | 18 | 14 | 512 | 13.6 | 6.1 | 93.1 | 16 | 5 |

[a]Complex points.
[b] Executed in three different versions to observe either histidine or tryptophan residues selectively or both in a single spectrum (see text).
[c] Phase cycling of $\phi_1$ (see Figure 4) has been omitted to allow acquisition with 16 transients per FID.

all cross peaks are aliased once, i.e. the apparent carrier position is shifted downfield from the water resonance by SW ($F_1$). The four-dimensional HC(C)NH–TOCSY$^{Trp}$ spectrum of xylanase was recorded at 500 MHz with spectral widths (number of complex data points, acquisition times) adjusted to 3.1 ppm (18, 10.8 ms), 19.0 ppm (14, 5.4 ms), 7.2 ppm (8, 19.2 ms) and 8.4 ppm (256, 61.0 ms) in the $t_1$ ($^1H^C$), $t_2$ ($^{13}C$), $t_3$ ($^{15}N$) and $t_4$ ($^1H^N$) dimensions, respectively. In this experiment phase cycling of $\phi_1$ was omitted, allowing to record only 16 scans per FID within a total measurement time of 94 h.

Two- and three-dimensional spectra were processed using the Bruker TopSpin 1.3 program. Processing of the 4D HC(C)NH–TOCSY$^{Trp}$ experiment was performed with the NMRPipe/NMRDraw software (Delaglio et al., 1995). In the latter data set, mirror-image linear prediction (Zhu and Bax, 1990) was employed to double the number of points in the $^{15}N$ dimension. In all other experiments time domain data in indirectly detected dimensions were typically extended by 1/4 to 1/3 of their original length. In the [$^{15}N$, $^1H$]–TROSY–H(NCDCG)CB and [$^{13}C$, $^1H$]–TROSY–HCD(CG)CB experiments (Löhr et al., 2002) linear prediction was employed to construct the missing first points in the $^{13}C^{\beta}$ dimensions to avoid large first-order phase corrections. Squared-cosine weighting functions were applied in all dimensions prior to zero-filling and Fourier transformation. Contour levels of all spectra displayed in the following are plotted on an exponential scale using a factor of $2^{1/2}$ in order to allow an approximate assessment of the obtained signal-to-noise ratios.

## Results and discussion

Using the methods proposed in this work, sequence-specific resonance assignments of all tryptophan and histidine ring protons and directly bound heteronuclei of a protein can be achieved in two steps. First, side-chain δ-protons or δ-carbons are linked to backbone amide protons and nitrogens of the following amino acid residue in H(CDCGCBCACO)NH or (H)CD(CGCBCACO)NH spectra, respectively. In the second step, connectivities between $^1H^{\delta}/^{13}C^{\delta}$ and the remaining $^1H$–$^{13}C$ spin pairs as well as the indole $^1H^{\varepsilon 1}$–$^{15}N^{\varepsilon 1}$ group are established with either (H)C(NC)H$^{His}$ or HC(C)NH–TOCSY$^{Trp}$ experiments. The only prerequisite is prior assignment of the signals in the [$^{15}N$, $^1H$]-HSQC spectrum by standard methods. Conversely, if backbone assignments still have to be obtained the present experiments provide amino acid type-selective correlations, indicating which signals in the HSQC originate from residues sequentially following either histidine or tryptophan (Schubert et al., 2001b).

The feasibility of the novel pulse sequences was first investigated with the medium-sized protein xylanase from *Bacillus agaradhaerens*, for which resonance assignments have been previously obtained (Betz et al., 2002; Löhr et al., 2002). Xylanase, which catalyses the degradation of xylan, one of the major constituents of plant cell walls (Sabini et al., 1999), consists of 207 amino acid residues (MW 23 kDa) including four histidines and seven tryptophans. To compare the different HCD(CGCBCACO)NH variants, a series of three 2D spectra was recorded, yielding amino-acid type selective $^1H$–$^{15}N$ correlation maps. Spectra resulting from His-, His/Trp- and Trp-selective experiments are shown in parts a–c of Figure 5. They contain all expected cross peaks, i.e. four at the positions of the residues sequentially following histidines and seven at the positions of the residues sequentially following tryptophans. An additional signal with a narrow line-shape in the proton dimension is observed in the His- and His/Trp-selective spectra and can be attributed to a small amount of a histidine-containing degradation product. Remarkably, no signal originating from other amino acid types, including phenylalanine and tyrosine, is detected in any of the spectra. The discrimination between histidine and tryptophan correlations is less perfect but acceptable: Only the strongest signals within each group, His32 and Trp104, produced very weak cross peaks in the selective spectra of the respective other amino acid type. The intensity of the former is 1/9 compared to its intensity in the His-selective spectrum and the intensity of the latter amounts to 1/6 of the intensity observed in the Trp-selective spectrum. This kind of 'cross-talk' is of course not relevant for the His/Trp-selective version, where both amino acid types are detected simultaneously and can be distinguished on the basis of opposite cross peaks signs. However, because of a compromise that must be made with respect to the offset of the

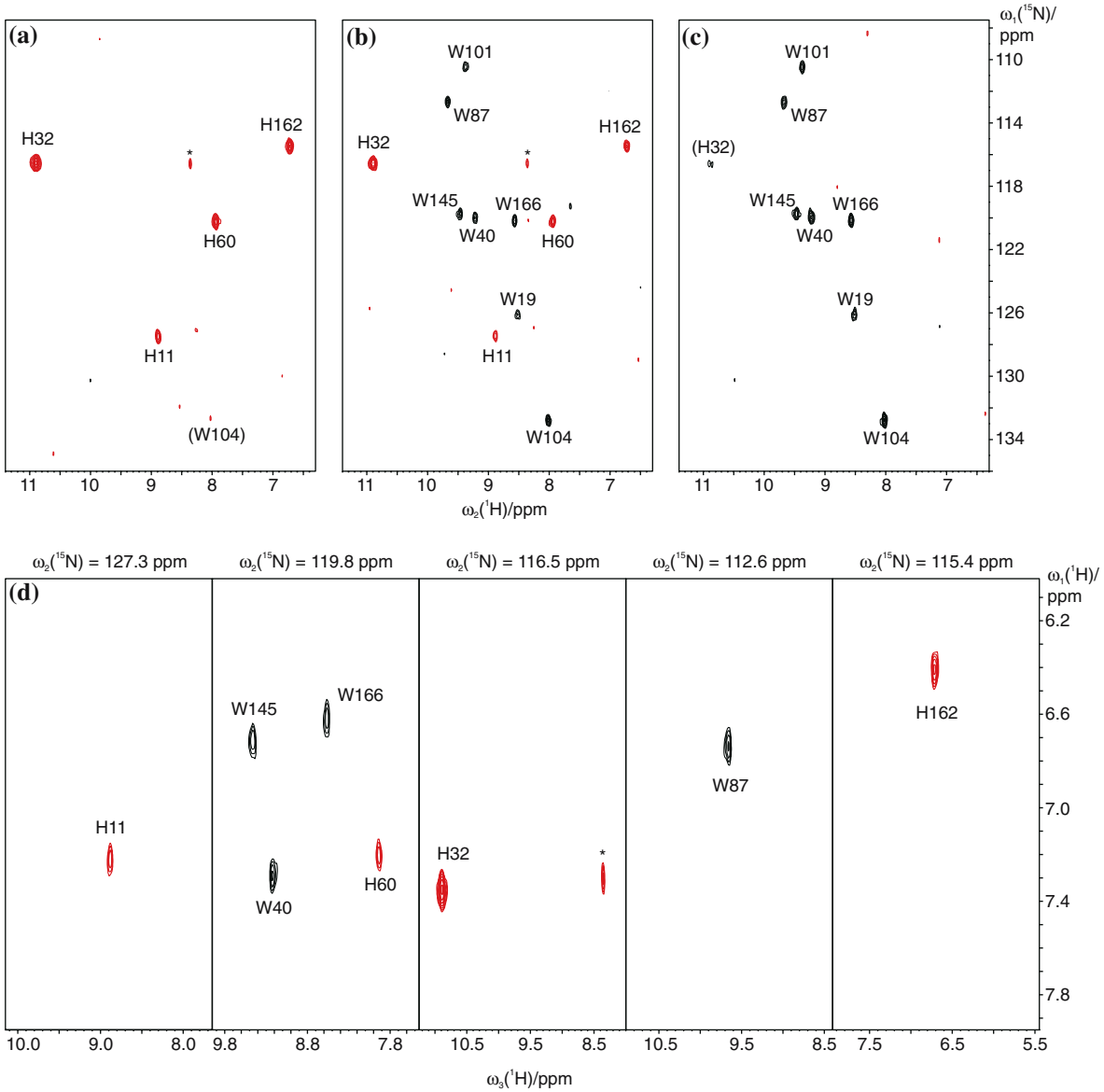


*Figure 5*. Two-dimensional (a) His-, (b) His/Trp- and (c) Trp-selective (HCDCGCBCACO)NH spectra (12 h measurement time each) of 1.3 mM xylanase and (d) $F_1$-$F_3$ ($^1H^{\delta}$–$^1H^{N}$) strips from a three-dimensional His/Trp-selective H(CDCGCBCACO)NH version (69 h measurement time), taken at the $^{15}N$ chemical shifts indicated above each slice. Positive and negative intensities are represented by black and red contours, respectively. The lowest contours in a–c are drawn close to the noise level to enable assessement of the selectivitiy for amino acid types. Peaks are labelled with the type and sequence number of the residue preceding the one whose amide $^{15}N$ and $^1H$ chemical shifts are detected. Labels in parenthesis indicate leakage signals of the respective other residue type in the His- and Trp-selective versions. Asterisks denote cross peaks due to a histidine-containing degradation product.

$^{13}C^{\gamma}$-selective inversion pulses in the sequence of Figure 2, the sensitivity of this variant is slightly lower than that of the Trp-selective version while the highest overall intensity is obtained in the His-selective version due the shorter ζ delay. The utility of the 3D H(CDCGCBCACO)NH experiment for the sequence-specific assignment of both histidine and tryptophan δ-protons of xylanase is demonstrated in Figure 5d. These chemical shifts serve as a starting point to assign the remaining ring protons and attached heteronuclei as described in the following sections.

The 2D (H)C(NC)$H^{His}$ experiment directly connects the $^1H^{\varepsilon 1}/^{13}C^{\varepsilon 1}$ pairs to the previously

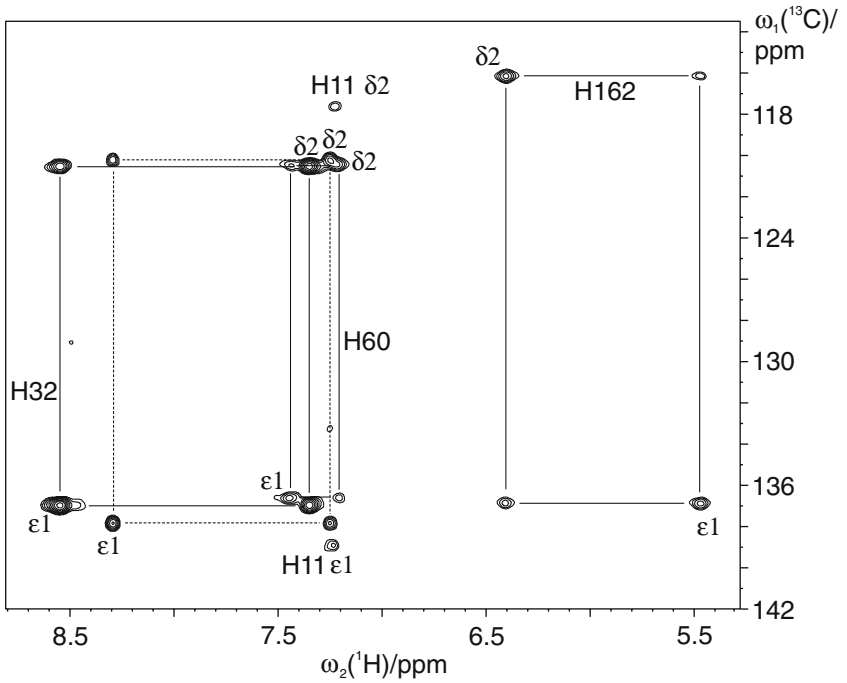


*Figure 6*. (H)C(NC)H$^{His}$ spectrum of xylanase recorded within 9 h at 500 MHz $^{1}$H frequency . The rectangular pattern of cross-/autocorrelation peaks of each imidazole ring is marked by vertical and horizontal lines and labelled with the residue number. Auto peaks ($^{1}H^{\delta2}/^{13}C^{\delta2}$ and $^{1}H^{\varepsilon1}/^{13}C^{\varepsilon1}$) are denoted with greek letters. For His11 only two peaks are observed due to $^{1}$H chemical shift degeneracy. Dashed lines connect signals arising from a histidine residue of degraded protein.

assigned $^{1}H^{\delta2}$ and/or $^{13}C^{\delta2}$ resonances without relying on common scalar correlations with intervening $^{15}$N nuclei as in alternative methods (Pelton et al., 1993; Sudmeier et al., 1996). Its application to xylanase is depicted in Figure 6. Each histidine residue is expected to give rise to a rectangular pattern consisting of the $^{1}H^{\varepsilon1}/^{13}C^{\varepsilon1}$ and $^{1}H^{\delta2}/^{13}C^{\delta2}$ autocorrelation peaks and two cross peaks sharing the $F_2(^{1}H)$ coordinate with the former and the $F_1(^{13}C)$ with the latter and vice versa, thus providing the desired linkage. Such patterns are easily identified for His32, His60 and His162 and in addition for the degradation product already observed in the H(CDCGCBCACO)NH spectra of Figure 5. At pH 5.3, where the measurement was carried out, the $^{1}H^{\delta2}$ and $^{1}H^{\varepsilon1}$ resonances of the fourth histidine residue (His11) are almost exactly degenerate (Betz et al., 2004). Therefore cross peaks superimpose with the two auto peaks at the common $^{1}$H chemical shift. Histidine-162 represents one of the rare cases where the $^{1}H^{\varepsilon1}$ chemical shift is upfield from that of $^{1}H^{\delta2}$. This is clearly confirmed by its relative signal intensities since the transfer period ε in the (H)C(NC)H$^{His}$ pulse sequence was adjusted to a value (17.2 ms) where autocorrelation peaks are stronger than the corresponding cross peaks. No signals from any other aromatic residue were detected in the (H)C(NC)H$^{His}$ spectrum of xylanase.

Assignment of indole ring proton and carbon resonances of tryptophan side chains in HCCH–COSY and HCCH–TOCSY spectra is often hampered by signal overlap which is aggravated by the presence of diagonal peaks. As a remedy, the HC(C)NH–TOCSY$^{Trp}$ experiment provides tryptophan-selective subspectra of the aromatic region void of diagonal peaks. Two options exist for the link to the non-aromatic portion of the tryptophan spin system, ensuring sequence-specific assignments: If $^{1}H^{\delta1}$ or $^{13}C^{\delta1}$ resonances have been assigned via HCD(CGCBCACO)NH experiments they can be matched with the corresponding cross peaks in HC(C)NH–TOCSY$^{Trp}$ spectra. Alternatively, $^{1}H^{\varepsilon1}/^{15}N^{\varepsilon1}$ chemical shifts obtained from, e.g., a [$^{15}$N, $^{1}$H]-TROSY-HN(CDCG)CB experiment (Löhr et al., 2002) may provide the pivot for correlations with aromatic $^{1}H$–$^{13}C$ groups. Figure 7 shows how all $^{1}H^{\varepsilon1}/^{15}N^{\varepsilon1}$,

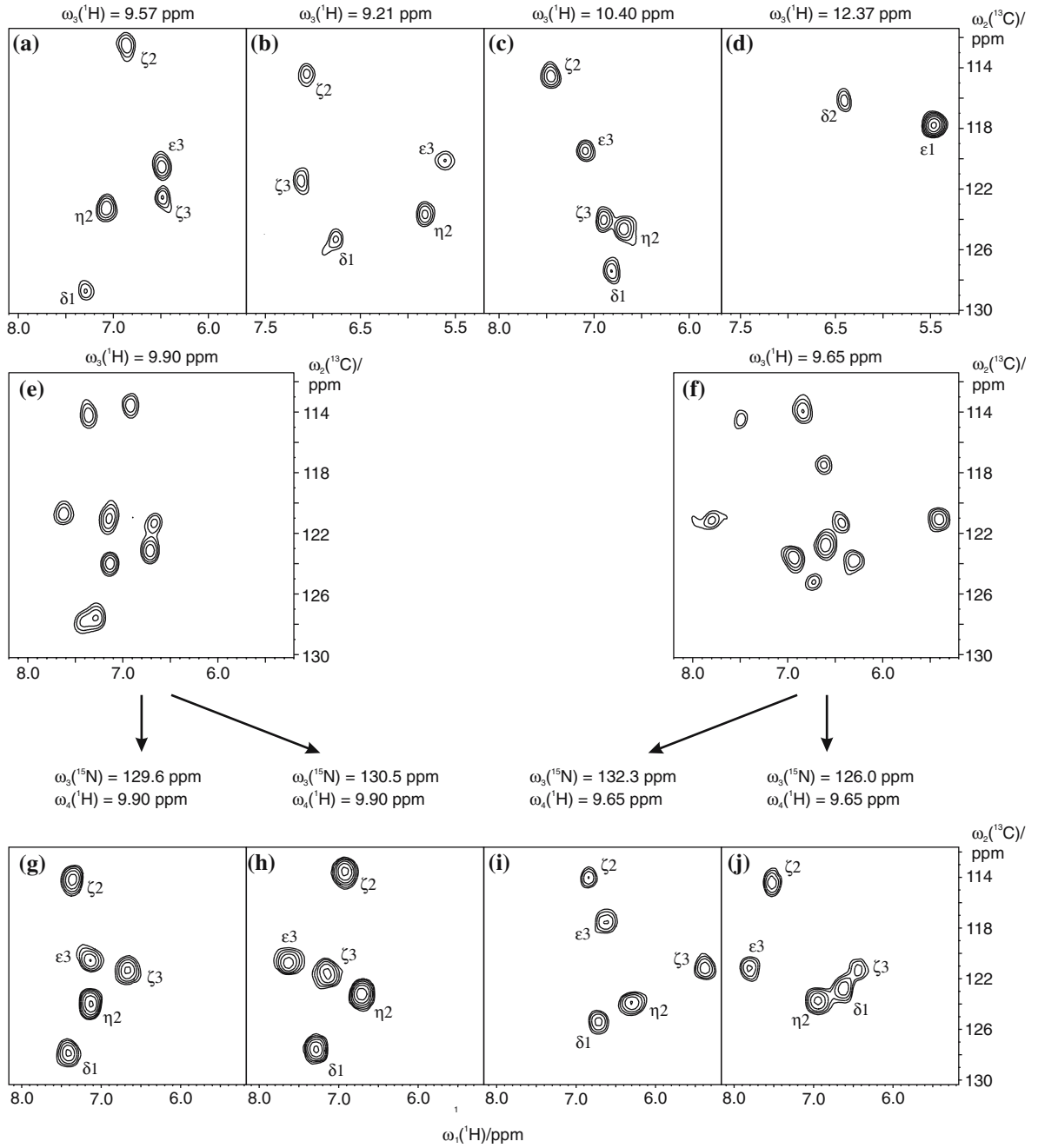


*Figure 7*. Complete resonance assignment of indole CH groups of the seven tryptophan residues in xylanase. $F_1$–$F_2$ ($^1$H–$^{13}$C) planes from (a–f) 3D HC(CN)H–TOCSY$^{Trp}$ and (g–j) 4D HC(C)NH–TOCSY$^{Trp}$ spectra are extracted at the $F_3$ ($F_3$ and $F_4$ in the case of the 4D version) positions given above each plot which correspond to the $^1H^{\varepsilon 1}$ ($^{15}N^{\varepsilon 1}$ and $^{15}H^{\varepsilon 1}$) chemical shifts of (a) Trp40, (b) Trp87, (c) Trp101, (e) Trp19/Trp104, (f) Trp145/Trp166, (g) Trp19, (h) Trp104, (i) Trp145 and (j) Trp166. Both experiments were acquired at 500 MHz, requiring 48 h measurement time for the 3D and 94 h for the 4D spectrum. Site-specific assignments are indicated by greek letters. The slice shown in (d) is taken at the $^1H^{\varepsilon 2}$ chemical shift of His162 whose $^{13}C^{\varepsilon 1}$ nucleus resonates at 136.9 ppm and therefore appears aliased once in the $F_2$ dimension.

$^{1}H^{\delta1}/^{13}C^{\delta1}$, $^{1}H^{\zeta2}/^{13}C^{\zeta2}$, $^{1}H^{\eta2}/^{13}C^{\eta2}$, $^{1}H^{\varepsilon3}/^{13}C^{\varepsilon3}$ and $^{1}H^{\zeta3}/^{13}C^{\zeta3}$ resonances of the seven tryptophan residues of xylanase were assigned sequence-specifically using the HC(C)NH–TOCSY$^{Trp}$ method. For each residue five cross peaks are expected in individual $F_1$–$F_2$ ($^{1}H^{C}$–$^{13}C$) planes as is indeed observed for Trp40, Trp87 and Trp101 in the 3D HC(CN)H–TOCSY$^{Trp}$ spectrum (Figure 7a–c). In contrast, more correlations are found in the slices at $^{1}H^{N}$ ($F_3$) chemical shifts of 9.65 and 9.90 ppm because Trp145 and Trp166 as well as Trp19 and Trp104 have nearly identical ε1-proton chemical shifts. Sequence-specific assignments are therefore impossible, and in addition overlap of cross peaks from different residues may occur as is the case for the pair Trp19/Trp104 where only eight rather than ten resolved signals are detected. This calls for introduction of a fourth dimension which is easily achieved by incrementing $t_3$ in the pulse sequence of Figure 4. Owing to the dispersion of the $^{15}N^{\varepsilon1}$ chemical shifts the corresponding $F_1$–$F_2$ planes from the 4D HC(C)NH–TOCSY$^{Trp}$ spectrum (Figure 7g–j) allow unambiguous identification of the five $^{1}H^{C}$–$^{13}C$ correlations for each of the four tryptophan residues, revealing the partial overlap of $^{1}H^{\delta1}$–$^{13}C^{\delta1}/^{1}H^{\delta1}$–$^{13}C^{\delta1}$ and $^{1}H^{\varepsilon3}$–$^{13}C^{\varepsilon3}/^{1}H^{\zeta3}$–$^{13}C^{\zeta3}$ cross peaks of the Trp19/Trp104 pair in the 3D version. This kind of overlap would inevitably cause ambiguities in the interpretation of HCCH–COSY and HCCH–TOCSY spectra as they exclusively rely on the dispersion of signals in the $^{1}H$–$^{13}C$ plane. It should be noted that because of the constant-time nature of the $^{15}N$ chemical shift evolution and the echo/antiecho type quadrature detection in the HC(C)NH–TOCSY$^{Trp}$ experiment no sensitivity loss is associated with the increased dimensionality, neglecting a minor line broadening due to the non-refocused $^{1}J_{N_{\varepsilon1}C_{\delta2}}$ interaction. Nevertheless, for most applications the 3D version provides sufficient dispersion of the indole $HN^{\varepsilon1}$ spectral region and is preferable since it requires less measurement times than the 4D for comparable resolution in the indirectly detected $^{1}H$ and $^{13}C$ dimensions.

A drawback of the HC(C)NH–TOCSY$^{Trp}$ method is the lack of information with respect to site-specific assignment. Almost invariably, $^{13}C^{\delta1}$ and $^{13}C^{\zeta2}$ have the most lowfield and highfield chemical shifts, respectively, of the protonated indole carbons. One of the rare exceptions is $^{13}C^{\delta1}$ of Trp166 in xylanase (see Figure 7j) which is unusually far upfield shifted. Such behaviour was not observed in any other tryptophan residue of the proteins studied here, in most cases allowing unambiguous assignments of these two moieties. Among the remaining carbon resonances the chemical shifts normally increase in the order $^{13}C^{\varepsilon3}$–$^{13}C^{\zeta3}$–$^{13}C^{\eta3}$, but their entire range spans less than 10 ppm according to the NMR database (BioMagResBank, http://www.bmrb.wisc.edu) (Seavey et al., 1991) such that occasional interchange cannot be ruled out. To gain more certainty about assignments of xylanase the HC(C)NH–TOCSY$^{Trp}$ experiment was also executed with a $^{13}C$ spin-lock time of only 5 ms (one cycle of FLOPSY-8), restricting the coherence transfer to not more than two steps. As a consequence, $^{1}H^{\delta1}$–$^{13}C^{\delta1}$ and $^{1}H^{\zeta3}$–$^{13}C^{\zeta3}$ cross peaks were not observed in the spectrum (results not shown), immediately revealing their positions by comparison with the spectra depicted in Figure 7. Apart from tryptophan side-chains, correlations can also be observed for histidine residues featuring slow-exchanging nitrogen bound protons as depicted in Figure 7d for His162 of xylanase. This is possible because their $^{13}C^{\varepsilon1}$ chemical shifts often lie close to those of tryptophan $^{13}C^{\varepsilon2}$ that are selected after the CC–TOCSY period in the HC(C)NH–TOCSY$^{Trp}$ pulse sequence. Interestingly, a $^{1}H^{\delta2}$–$^{13}C^{\delta2}$ cross peak is detected, too, indicating that the imidazole ring $^{2}J_{C_{\delta2}C_{\varepsilon1}}$ and/or $^{3}J_{C_{\delta2}C_{\varepsilon1}}$ coupling constants are large enough to ensure magnetization transfer during the 10-ms mixing time.

As mentioned above, sequence specific assignments of aromatic residues based on correlations with β-carbons might fail if the latter resonances do not provide sufficient dispersion. Such a case was encountered for the 120-residue amino-terminal domain of human Cdc5 for which NMR-based structural studies are currently being pursued in our laboratory. hCdc5 specifically binds to DNA and is assumed to regulate G2/M through transcriptional activation (Lei et al., 2000). It contains six tryptophan residues one of which gives a very weak $^{1}H^{\varepsilon1}$–$^{15}N^{\varepsilon1}$ cross peak in a standard HSQC spectrum and was not observed in any other experiment recorded in this study. Of the remaining five ε1-protons, four showed intraresidual correlations to β-carbons resonating within 0.5 ppm in a 2D [$^{15}N$, $^{1}H$]–TROSY–H(NCDCG)CB spectrum (Figure 8a). While it should in principle be possible

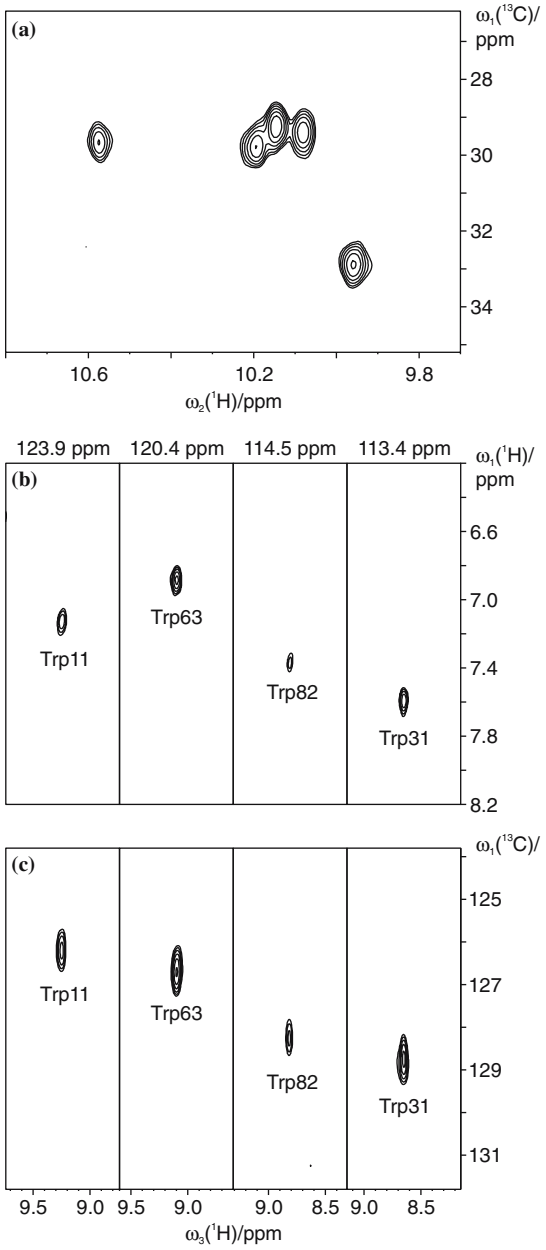


*Figure 8*. Sequence-specific assignment of tryptophan side-chain resonances of hCdc5 (0.6 mM sample concentration). (a) $^{1}H^{\varepsilon 1}$–$^{13}C^{\beta}$ correlations obtained in a 2D [$^{15}N$, $^{1}H$]-TROSY-H(NCDCG)CB spectrum show little dispersion of $^{13}C^{\beta}$ chemical shifts for most signals, preventing unambiguous assignments. $F_1$–$F_3$ strips from Trp-selective (b) 3D H(CDCGCBCACO)NH and (c) 3D (H)CD(CGCBCACO)NH spectra, taken at the $^{15}N$ ($F_2$) chemical shifts indicated at the top of panel b. Here, sequential assignments are based on correlations between $^{1}H^{\delta 1}$ or $^{13}C^{\delta 1}$ and backbone amide $^{1}H/^{15}N$ resonances of the respective following residue. Spectra were recorded at 600 MHz using a room-temperature probe for the [$^{15}N$, $^{1}H$]-TROSY-H(NCDCG)CB experiment and a cryogenic probe for the two HCD(CGCBCACO)NH experiments.

to link the detected indole protons to the backbone unless two or more $^{13}C^{\beta}$ resonances are completely degenerate we were unable to obtain unambigous assignments from this experiment because none of the observed chemical shifts exactly matched those extracted from a 3D [$^{15}N$,$^{1}H$]-TROSY-HNCACB (Wittekind and Mueller, 1993; Salzmann et al., 1999) spectrum which had been recorded on a different sample of the same protein. These problems are obviously avoided when aromatic chemical shifts are directly correlated with the backbone in a single experiment rather than in the $^{13}C^{\beta}$ mediated manner. Each of the four tryptophan residues which could not be differentiated in the H(NCDCG)CB / HNCACB combination gives rise to well resolved cross peaks at unique amide $^{1}H$ and $^{15}N$ chemical shifts in either 3D H(CDCGBCACO)NH (Figure 8b) or 3D (H)CD(CGCBCACO)NH (Figure 8c) spectra. It should be pointed out that in general it is neither necessary nor desirable to record both versions or, alternatively, combine them in a four-dimensional version in order to obtain both $^{1}H^{\delta}$ and $^{13}C^{\delta}$ chemical shifts since one can normally retrieve the other in a simple [$^{13}C$, $^{1}H$]-HSQC or -TROSY experiment once one of them has been assigned.

In an analogous manner, assignment of histidine ring resonances based on $^{13}C^{\beta}$–$^{1}H^{\delta 2}$ correlations may be obstructed by overlap. The situation can be aggravated by the presence of a His-tag. As an example, Figure 9a shows a 2D [$^{13}C$, $^{1}H$]-TROSY-H(CDCG)CB spectrum of RcsC-PR which comprises amino acids 684–933 of the RcsC sensor kinase and a non-cleavable C-terminal $(His)_6$-tag. It is part of the signaling system in *E. coli* and receives a phosphoryl group from the histidine protein kinase domain and transfers it to a phosphotransferase domain. The native sequence of the 28-kDa RcsC-PR domain contains five histidine as well as three tryptophan residues. Very strong signals due to the His-tag clustering around random coil chemical shifts ($\approx$ 7.0/30.5 ppm in the $^{1}H/^{13}C$ dimensions) prevent unequivocal identification of the native histidine signals although some of them appear at least partially resolved. Introduction of a third dimension in the pulse sequence in order to additionally record aromatic $^{13}C$ chemical shifts, did not considerably improve the situation as $^{13}C^{\delta 2}$ resonances likewise show very poor dispersion (data not shown). In contrast, directly correlating $^{1}H^{\delta 2}$ with the backbone using

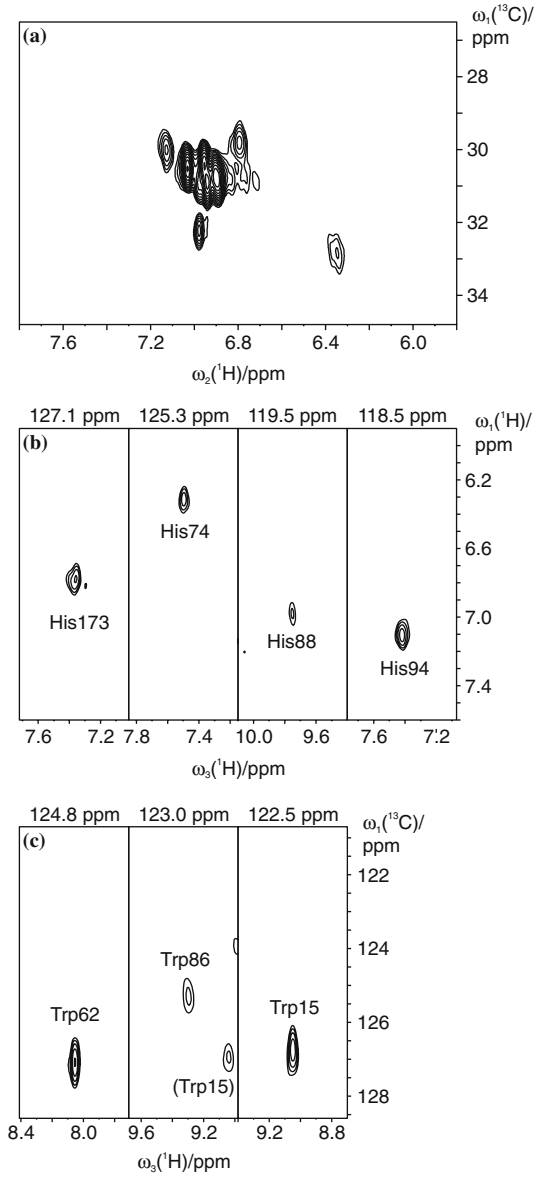


*Figure 9.* Assignment of histidine and tryptophan ring resonances of RcsC-PR. (a) In the 2D [$^{13}$C, $^{1}$H]-TROSY-H(CDCG)CB spectrum $^{1}H^{\delta 2}$–$^{13}C^{\beta}$ cross peaks of native histidine residues may by obscured by very strong signals from the His-tag. (b) Sequential $^{1}H^{\delta 2}$–$^{15}N/^{1}H^{N}$ connectivities are easily obtained from a His-selective 3D H(CDCGCBCACO)NH spectrum (measurement time: 72 h). (c) Expansions from $F_1$–$F_3$ slices of a Trp-selective 3D (H)CD(CGCBCACO)NH spectrum (measurement time: 84 h) showing $^{13}C^{\delta 1}$–$^{15}N$–$^{1}H^{N}$ correlations for each of the three tryptophan residues. In the strip taken at the $^{15}$N chemical shift of Trp86 (123.0 ppm) a weak cross peak of Trp15, which resonates 0.5 ppm upfield in the nitrogen dimension, is also observed. All spectra were collected at a 600 MHz spectrometer using a 0.8 mM sample of RcsC-PR.

the 3D H(CDCGBCACO)NH sequence benefits from the higher resolution in the $^{1}$H–$^{15}$N plane, usually resulting in cross peaks well separated from those of the His-tag residues, as is verified in Figure 9b. A further advantage of the $H^N$ detected experiment which applies here, is that signals from the latter residues are often attenuated due to rapid exchange with the solvent. Unfortunately, one of the histidine residues of RcsC-PR is followed by a proline such that only four out of five could be sequentially assigned in this manner. A potential solution to this problem would be an alternative H(CDCGCBCA)NH sequence, where magnetization is not relayed via $^{13}$C' spins but directly transferred from α-carbons to the amide group of the same amino acid residue. However, it can be expected that such an experiment would be less sensitive due to smaller coupling constants employed for coherence transfer and the presence of passive $^{2}J_{NC\alpha}$ interactions. Also presented (Figure 9c) is the assignment of the three tryptophan residues from a 3D (H)CD(CGCBCACO)NH spectrum. Intensities of Trp86 as well as His88 correlations are strikingly low compared to those of the remaining histidine and tryptophan residues. They are located in a proline-rich loop region that yields bad signal-to-noise ratios in standard triple-resonance experiments employed for backbone assignment, too. The most likely reason is fast transverse relaxation due to conformational exchange. Further indole ring system $^{1}$H and $^{13}$C assignments of RcsC-PR are based on the $^{13}C^{\delta 1}$ resonances identified in the 3D (H)CD(CGCBCACO)NH spectrum of Figure 9c. Each of the three $F_1$–$F_2$ planes from the 3D HC(CN)H–TOCSY$^{Trp}$ spectrum (Figure 10) contains the five expected correlations. Since the $^{1}H^{\varepsilon 1}$ chemical shifts are more distinctive than in xylanase, a four-dimensional version was not required here. Tentative site-specific assignments indicated in Figure 10 are supported by the disappearance of $^{1}H^{\delta 1}$–$^{13}C^{\delta 1}$ and $^{1}H^{\zeta 3}$–$^{13}C^{\zeta 3}$ cross peaks in a HC(CN)H–TOCSY$^{Trp}$ spectrum recorded with a 5-ms $^{13}$C spin-lock time (data not shown).

With the exception of the 4D HC(C)NH–TOCSY$^{Trp}$ of xylanase, where the relatively long recording time of almost 4 days is a result of the high dimensionality, the time requirements for all spectra shown so far were governed by sensitivity. The magnetization transfer pathways induced by the three pulse sequences developed here involve

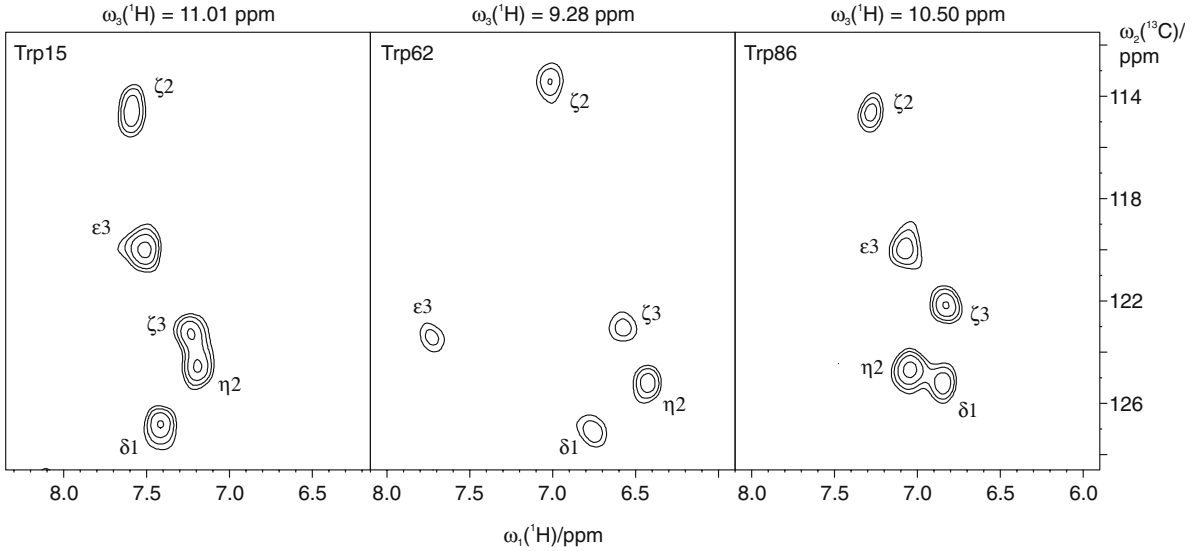


*Figure 10*. $F_1$–$F_2$ planes from a 3D HC(CN)H–TOCSY$^{Trp}$ spectrum of RcsC-PR taken at the $^1H^{\varepsilon 1}$ chemical shifts of Trp15, Trp62 and Trp86 as indicated at the top of each plot. Data acquisition required 59 h on a 500 MHz spectrometer.

multiple relay steps. As a consequence, long overall delay periods render the experiments highly susceptiple to transverse relaxation. Therefore, since sample deuteration is not an option, they are clearly not suitable for larger proteins. Signal-to-noise ratios obtained for RcsC-PR with an overall correlation time of 18 ns, estimated from its number of amino acid residues and the sample temperature using an empirical equation (Daragan and Mayo, 1997), suggest that 25–30 kDa represent the upper limit for the molecular weight of proteins to which the new methods can be applied successfully. Surprisingly, the DNA binding domain of hCdc5, which has a molecular weight of 14 kDa, was the only protein used in this study where the sensitivity of spectrometers equipped with room-temperature probes was not sufficient and experiments had to be carried out with a cryogenically cooled probe. This cannot be explained by the somewhat lower sample concentration alone. Although $T_2$ times remain to be determined, line widths observed in a standard [$^{15}$N, $^1$H]-HSQC spectrum are unusually large for a protein of that size. A possible reason could be partial aggragation or the formation of a dimeric state in equilibrium with monomers at the concentration employed here.

On the other hand, under favourable conditions (low molecular weight, no aggragation, high sample concentrations) the novel pulse sequences are quite efficient. This is demonstrated in Figure 11 for the proteins ribonuclease T1 (11 kDa) and flavodoxin (16 kDa). In both cases it was sufficient to record two-dimensional H(CDCGCBCACON)H or (H)CD(CGCBCACON)H spectra in order to achieve the aromatic-to-backbone link because of the low number of histidine and tryptophan residues and the non-degeneracy of amide proton chemical shifts of the respective following amino acid residue. The sole tryptophan residue in RNase T1 is sequentially followed by a proline such that no correlation can be obtained here. Based on the resulting δ-proton or -carbon chemical shifts the histidine $^1H^{\varepsilon 1}/^{13}C^{\varepsilon 1}$ and tryptophan $^1H^{\zeta 2}/^{13}C^{\zeta 2}$, $^1H^{\eta 2}/^{13}C^{\eta 2}$, $^1H^{\varepsilon 3}/^{13}C^{\varepsilon 3}$, $^1H^{\zeta 3}/^{13}C^{\zeta 3}$ and $^1H^{\varepsilon 1}/^{15}N^{\varepsilon 1}$ resonances of the two proteins are then sequentially assigned from 2D (H)C(NC)H$^{His}$ and 3D HC(CN)H–TOCSY$^{Trp}$ spectra, respectively.

In the (H)C(NC)H$^{His}$ experiment on flavodoxin the imidazole-selective shaped 180° $^{15}$N pulses in the $T_C$ and ζ periods were replaced by non-selective rectangular pulses such that $^1H^{\delta 1}/^{13}C^{\delta 1}$ autocorrelation peaks of tryptophans are detected, too, yielding the chemical shifts of the protons bound to the δ1-carbons identified from the (H)CD(CGC BCACON)H, without the need to take an additional [$^{13}$C,$^1$H]-HSQC or -TROSY spectrum. Site

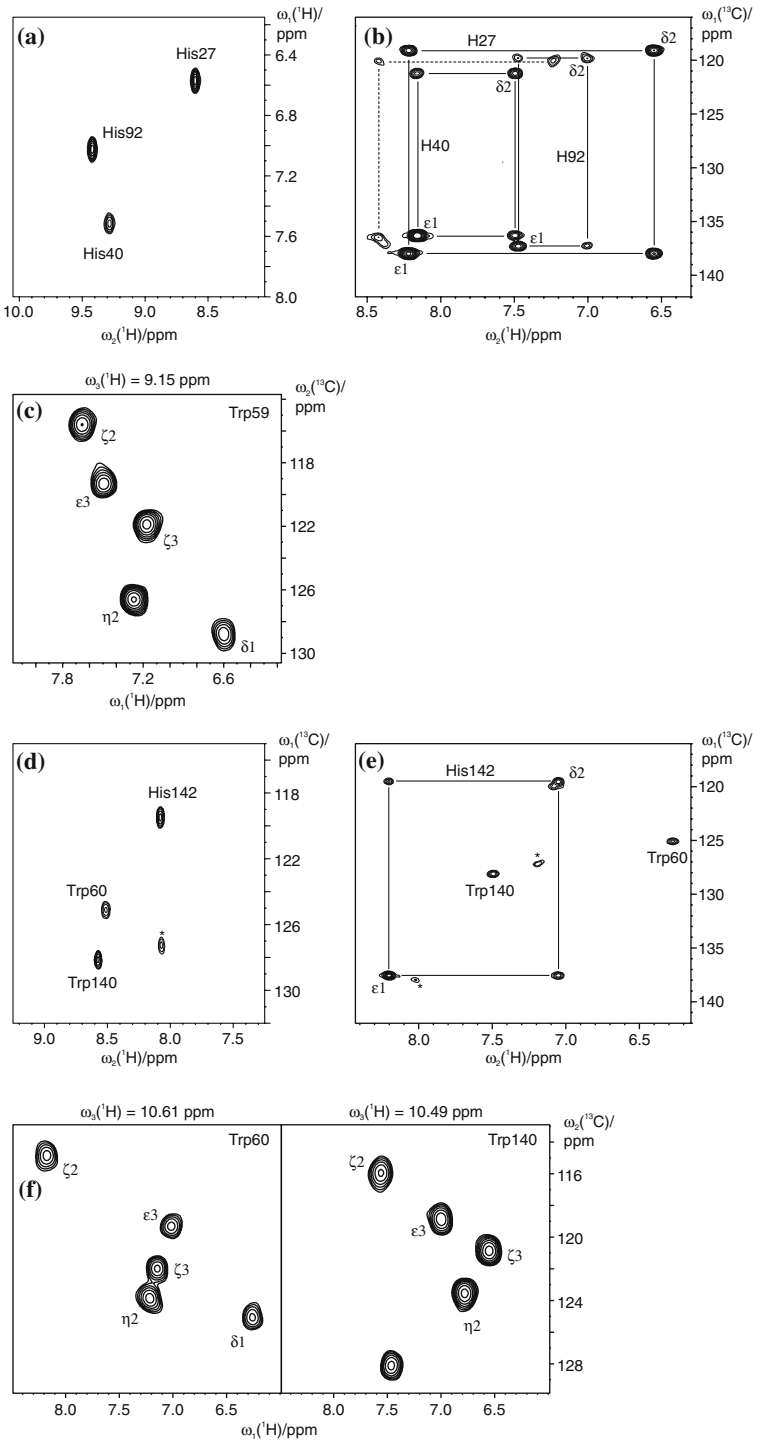


*Figure 11.* Application of the three pulse sequences described in this paper to (a–c) RNase T1 (2 mM sample concentration) and (d–f) *Desulfovibrio vulgaris* flavodoxin (2.1 mM sample concentration). Shown are regions from (a) 2D His-selective H(CDCGCBCACON)H and (d) 2D Trp/His-selective (H)CD(CGCBCACON)H spectra, (b, e) 2D (H)C(NC)H$^{His}$ spectra and (c, f) $F_1$–$F_2$ planes from 3D HC(CN)H–TOCSY$^{Trp}$ spectra, all acquired at 500 MHz $^1$H frequency. Positive and negative intensities in spectrum d, where histidine and tryptophan signals have opposite signs, are plotted without distinction. Cross peaks connected by dashed lines in the (H)C(NC)H$^{His}$ spectrum b arise from a small fraction of denatured protein as previously observed for other preparations of RNase T1 (Schmidt et al., 1991; Spitzner et al., 2001). In the spectra of flavodoxin, signals due to degradation products are labelled with asterisks.

specific indole ring assignments are in accordance with aromatic proton chemical shifts from previous homonuclear correlation experiments (Hoffmann and Rüterjans, 1988; Knauf et al., 1993). The total measurement time for the set of three experiments on RNase T1 and flavodoxin was only about 7 h each, using a moderate static field (500 MHz) and conventional triple-resonance probes, showing that for 'well-behaving' proteins sensitivity is not a limitation of the described methods.

## Conclusions

A procedure has been proposed to assign all aromatic $^{1}H$–$^{13}C$ pairs and the indole $^{1}H$–$^{15}N$ group of histidine and tryptophan residues in small to medium sized proteins. Either $^{1}H^{\delta}$ or $^{13}C^{\delta}$ are correlated with backbone chemical shifts via H(CDCGCBCACO)NH / (H)CD(CGCBCACO)NH experiments. Optionally, selective versions of the pulse sequences can be used that are slightly more sensitive but provide the connectivities only for one of the two residue types. The obtained sequence-specific $^{1}H^{\delta}/^{13}C^{\delta}$ resonance assignments are then extended to the benzene moiety of the indole ring system of tryptophan side chains using a HC(C)NH–TOCSY type pulse sequence while they are linked to the $^{1}H^{\varepsilon}$–$^{13}C^{\varepsilon}$ group of histidines by two successive polarization transfer steps across the intervening nitrogen nucleus. Taking advantage of the dispersion of backbone amide or indole $^{1}H$–$^{15}N$ resonances, HCD(CGCBCAC-O)NH and HC(C)NH-TOCSY$^{Trp}$ experiments usually result in well-resolved spectra and circumvent problems due to crowding in the $^{13}C^{\beta}$ region or overlap with His-tag signals as in previously proposed methods.

The performance of the pulse sequences is found to be strongly dependent on the relaxation properties of the protein to which they are applied. While excellent sensitivity can be achieved for small proteins, increasing rotational correlation times require longer instrumental times and/or use of cryogenically cooled probes. Analogous to other triple-resonance methods, the new experiments allow aromatic chemical shift assignments to be established independently of NOE information. This helps reducing errors that sometimes occur when resonances are assigned from the same spectra used to derive structural constraints.

## Acknowledgements

The authors would like to thank Marco Betz, Gary Yalloway and Norman Spitzner for the preparation of xylanase, flavodoxin and RNase T1 samples, respectively. Recombinant xylanase was produced in collaboration with Novo-Nordisk A/S (Bagsvaerd, Denmark). Financial support from the Deutsche Forschungsgemeinschaft (BE 1911/4-1) is gratefully acknowledged. The Centre for Biomolecular Magnetic Resonance is supported by the state of Hesse.

## References

Alei, M. Jr., Morgan, L.O., Wageman, W.E. and Whaley, T.W. (1980) *J. Am. Chem. Soc.* **102**, 2881–2887.
Bax, A., Clore, G.M., Driscoll, P.C., Gronenborn, A.M., Ikura, M. and Kay, L.E. (1990a) *J. Magn. Reson.* **87**, 620–627.
Bax, A., Clore, G.M. and Gronenborn, A.M. (1990b) *J. Magn. Reson.* **88**, 425–431.
Bax, A. and Grzesiek, S. (1993) *Acc. Chem. Res.* **26**, 131–138.
Bax, A., Sparks, S.W. and Torchia, D.A. (1988) *J. Am. Chem. Soc.* **110**, 7926–7927.
Betz, M., Löhr, F., Wienk, H. and Rüterjans, H. (2002) *J. Biomol. NMR* **23**, 333–334.
Betz, M., Löhr, F., Wienk, H. and Rüterjans, H. (2004) *Biochemistry* **43**, 5820–5831.
Billeter, M., Braun, W. and Wüthrich, K. (1982) *J. Mol. Biol.* **155**, 321–346.
Blomberg, F., Maurer, W. and Rüterjans, H. (1977) *J. Am. Chem. Soc.* **99**, 8149–8159.
Boyd, J. and Soffe, N. (1989) *J. Magn. Reson.* **85**, 406–413.
Brutscher, B., Boisbouvier, J., Pardi, A., Marion, D. and Simorre, J.-P. (1998) *J. Am. Chem. Soc.* **120**, 11845–11851.
Cavanagh, J., Fairbrother, W.J., Palmer, A.G. III and Skelton, N.J. (1996) *Protein NMR Spectroscopy Principles and Practice*, Academic Press, Inc., San Diego.
Cavanagh, J., Palmer, A.G. III, Wright, P.E. and Rance, M. (1991) *J. Magn. Reson.* **91**, 429–436.
Carlomagno, T., Maurer, M., Sattler, M., Schwendinger, M.G., Glaser, S.J. and Griesinger, C. (1996) *J. Biomol. NMR* **8**, 161–170.
Daragan, V.A. and Mayo, K.H. (1997) *Prog. Nucl. Magn. Res. Spectrosc.* **31**, 63–105.
Delaglio, F., Grzesiek, S., Vuister, G.W., Zhu, G., Pfeifer, J. and Bax, A. (1995) *J. Biomol. NMR* **6**, 277–293.
Emsley, L. and Bodenhausen, G. (1990) *Chem. Phys. Lett.* **165**, 469–476.
Fesik, S.W., Eaton, H.L., Olejniczak, E.T., Zuiderweg, E.R.P., McIntosh, L.P. and Dahlquist, F.W. (1990) *J. Am. Chem. Soc.* **112**, 886–888.
Geen, H. and Freeman, R. (1991) *J. Magn. Reson.* **93**, 93–141.
Grzesiek, S. and Bax, A. (1992) *J. Am. Chem. Soc.* **114**, 6291–6293.
Grzesiek, S., Anglister, J. and Bax, A. (1993) *J. Magn. Reson. B* **101**, 114–119.
Grzesiek, S. and Bax, A. (1993a) *J. Am. Chem. Soc.* **115**, 12593–12594.

Grzesiek, S. and Bax, A. (1993b) *J. Biomol. NMR* **3**, 185–204.
Grzesiek, S. and Bax, A. (1995) *J. Am. Chem. Soc.* **117**, 6527–6531.
Hoffmann, E. and Rüterjans, H. (1988) *Eur. J. Biochem.* **177**, 539–560.
Jahnke, W. and Kessler, H. (1994) *J. Biomol. NMR* **4**, 735–740.
Kay, L.E. (1995) *Prog. Biophys. Molec. Biol.* **63**, 277–299.
Kay, L.E., Ikura, M. and Bax, A. (1990) *J. Am. Chem. Soc.* **112**, 888–889.
Kay, L.E., Keifer, P. and Saarinen, T. (1992) *J. Am. Chem. Soc.* **114**, 10663–10665.
Knauf, M., Löhr, F., Curley, G.P., O'Farrell, P., Mayhew, S.G., Müller, F. and Rüterjans, H. (1993) *Eur. J. Biochem.* **213**, 167–184.
Kupče, Ē., Boyd, J. and Campbell, I.D. (1995) *J. Magn. Reson.* **B106**, 300–303.
Lei, X.-H., Shen, X, Xu, X.-Q. and Bernstein, H.S. (2000) *J. Cell Sci.* **113**, 4523–4531.
Lippens, G., Dhalluin, C. and Wieruszeski, J.-M. (1995) *J. Biomol. NMR* **5**, 327–331.
Logan, T.M., Olejniczak, E.T., Xu, R.X. and Fesik, S.W. (1992) *FEBS Lett.* **314**, 413–418.
Logan, T.M., Olejniczak, E.T., Xu, R.X. and Fesik, S.W. (1993) *J. Biomol. NMR* **3**, 225–231.
Löhr, F., Katsemi, V., Betz, M., Hartleib, J. and Rüterjans, H. (2002) *J. Biomol. NMR* **22**, 153–164.
Löhr, F. and Rüterjans, H. (1996) *J. Magn. Reson.* **B112**, 259–268.
Lyons, B.A. and Montelione, G.T. (1993) *J. Magn. Reson.* **B101**, 206–209.
Marion, D., Ikura, M., Tschudin, R. and Bax, A. (1989) *J. Magn. Reson.* **85**, 393–399.
Matsuo, H., Kupče, Ē., Li, H. and Wagner, G. (1996) *J. Magn. Reson.* **B111**, 194–198.
Mohebbi, A and Shaka, A.J. (1991) *Chem. Phys. Lett.* **178**, 374–378.
Montelione, G.T., Lyons, B.A., Emerson, S.D. and Tashiro, M. (1992) *J. Am. Chem. Soc.* **114**, 10974–10975.
Morris, G.A. and Freeman, R. (1979) *J. Am. Chem. Soc.* **101**, 760–762.
Muhandiram, D.R. and Kay, L.E. (1994) *J. Magn. Reson.* **B 103**, 203–216.
Otting, G. and Liepinsh, E. (1995) *J. Biomol. NMR* **5**, 420–426.
Patt, S. (1992) *J. Magn. Reson.* **96**, 94–102.
Pelton, J.G., Torchia, D.A., Meadow, N.D. and Roseman, S. (1993) *Protein Sci.* **2**, 543–558.
Pervushin, K., Riek, R., Wider, G. and Wüthrich, K. (1997) *Proc. Natl. Acad. Sci. USA* **94**, 12366–12371.
Pervushin, K., Riek, R., Wider, G. and Wüthrich, K. (1998) *J. Am. Chem. Soc.* **120**, 6394–6400.
Peti, W., Norcross, J., Eldridge, G. and O'Neill-Johnson, M. (2004) *J. Am. Chem. Soc.* **126**, 5873–5878.
Piotto, M., Saudek, V. and Sklenář, V. (1992) *J. Biomol. NMR* **2**, 661–665.
Prompers, J.J., Groenewegen, A., Schaik, R.C.van, Pepermans, H.A.M. and Hilbers, C. (1997) *Protein Sci.* **6**, 2375–2384.
Prompers, J.J., Groenewegen, A., Hilbers, C.W. and Pepermans, H.A.M. (1998) *J. Magn. Reson.* **130**, 68–75.
Rogov, V.V., Bernhard, F., Löhr, F. and Dötsch, V. (2004) *J. Mol. Biol.* **343**, 1035–1048.
Sabini, E., Sulzenbacher, G., Dauter, M., Dauter, Z., Jorgensen, P.L., Schulein, M., Dupont, C., Davies, G.J. and Wilson, K.S. (1999) *Chem. Biol.* **6**, 483–492.
Salzmann, M., Wider, G., Pervushin, K., Senn, H. and Wüthrich, K. (1999) *J. Am. Chem. Soc.* **121**, 844–848.
Schmidt, J.M., Thüring, H., Werner, A., Rüterjans, H., Quaas, R. and Hahn, U. (1991) *Eur. J. Biochem.* **197**, 643–653.
Schubert, M., Smalla, M., Schmieder, P. and Oschkinat, H. (1999) *J. Magn. Reson.* **141**, 34–43.
Schubert, M., Schmieder, P. and Oschkinat, H. (2001a) *J. Magn. Reson.* **148**, 61–72.
Schubert, M., Schmieder, P. and Oschkinat, H. (2001b) *J. Magn. Reson.* **153**, 186–192.
Seavey, B.R., Farr, E.A., Westler, W.M. and Markley, J.L. (1991) *J. Biomol. NMR* **1**, 217–236.
Shaka, A.J., Barker, P.B. and Freeman, R. (1985) *J. Magn. Reson.* **64**, 547–552.
Shaka, A.J., Lee, C.J. and Pines, A. (1988) *J. Magn. Reson.* **77**, 274–293.
Shimba, N., Serber, Z., Ledwidge, R., Miller, S.M., Craik, C.S. and Dötsch, V. (2003) *Biochemistry* **42**, 9227–9234.
Shimba, N., Takahashi, H., Sakakura, M., Fujii, I. and Shimada, I. (1998) *J. Am. Chem. Soc.* **120**, 10988–10989.
Sklenář, V., Peterson, R.D., Rejante, M.R., Wang, E. and Feigon, J. (1993a) *J. Am. Chem. Soc.* **115**, 12181–12182.
Sklenář, V., Piotto, M., Leppik, R. and Saudek, V. (1993b) *J. Magn. Reson.* **A102**, 241–245.
Spitzner, N., Löhr, F., Pfeiffer, S., Koumanov, A., Karshikoff, A. and Rüterjans, H. (2001) *Eur. Biophys. J.* **30**, 186–197.
Stonehouse, J., Shaw, G.L., Keeler, J. and Laue, E.D. (1994) *J. Magn. Reson. A* **107**, 178–184.
Sudmeier, J.L., Ash, E.L., Günther, U.L., Luo, X., Bullock, P.A. and Bachovchin, W.W. (1996) *J. Magn. Reson.* **B113**, 236–247.
Wagner, G. and Wüthrich, K. (1982) *J. Mol. Biol.* **155**, 347–366.
Wittekind, M. and Mueller, L. (1993) *J. Magn. Reson.* **B101**, 201–205.
Wüthrich, K. (1986) *NMR of Proteins and Nucleic Acids* Wiley, New York, NY.
Yamazaki, T., Forman-Kay, J.D. and Kay, L.E. (1993) *J. Am. Chem. Soc.* **115**, 11054–11055.
Zerbe, O., Szyperski, T., Ottiger, M. and Wüthrich, K. (1996) *J. Biomol. NMR* **7**, 99–106.
Zhu, G. and Bax, A. (1990) *J. Magn. Reson.* **90**, 405–410.